

# Fibration symmetry-breaking supports functional transitions in a brain network engaged in language

**Hernan Makse**

hmakse@ccny.cuny.edu

City College of New York <https://orcid.org/0000-0001-6474-1324>

**Tommaso Gili**

Networks Unit, IMT School for Advanced Studies Lucca <https://orcid.org/0000-0001-9154-1758>

**Bryant Avila**

City College of New York

**Luca Pasquini**

Memorial Sloan Kettering Cancer Center

**Andrei Holodny**

MSKCC <https://orcid.org/0000-0002-1159-2705>

**David Phillips**

University of New Mexico

**Paolo Boldi**

University of Milan <https://orcid.org/0000-0002-8297-6255>

**Andrea Gabrielli**

Dipartimento di Ingegneria, Università Roma 3

**Guido Caldarelli**

University of Venice <https://orcid.org/0000-0001-9377-3616>

**Manuel Zimmer**

Vienna Biocenter

---

**Physical Sciences - Article**

**Keywords:**

**Posted Date:** June 7th, 2024

**DOI:** <https://doi.org/10.21203/rs.3.rs-4409330/v1>

**License:**   This work is licensed under a Creative Commons Attribution 4.0 International License.

[Read Full License](#)

**Additional Declarations:** There is **NO** Competing Interest.

---

# Fibration symmetry-breaking supports functional transitions in a brain network engaged in language

Tommaso Gili<sup>1,2</sup>, Bryant Avila<sup>3</sup>, Luca Pasquini<sup>4,5</sup>, Andrei Holodny<sup>4,6,7</sup>, David Phillips<sup>8,9</sup>, Paolo Boldi<sup>10</sup>, Andrea Gabrielli<sup>11,12</sup>, Guido Caldarelli<sup>2,13,14</sup>, Manuel Zimmer<sup>15</sup> & Hernán A. Makse<sup>3,4</sup>

<sup>1</sup>*Networks Unit, IMT Scuola Alti Studi Lucca, Piazza San Francesco 15, 55100- Lucca, Italy.*

<sup>2</sup>*Institute for Complex Systems (ISC), CNR, UoS Sapienza, Rome, 00185, Italy.*

<sup>3</sup>*Levich Institute and Physics Department, City College of New York, New York, NY 10031, USA.*

<sup>4</sup>*Neuroradiology Service, Department of Radiology, Memorial Sloan Kettering Cancer Center, New York, NY 10065, USA.*

<sup>5</sup>*Neuroradiology Unit, NESMOS Department, Sant'Andrea Hospital, La Sapienza University, Rome, 00189, Italy.*

<sup>6</sup>*Department of Neurology and Neuroscience, Weill Medical College of Cornell University, New York, NY, 10021, USA.*

<sup>7</sup>*Department of Radiology, Weill Medical College of Cornell University, New York, NY 10065, USA.*

<sup>8</sup>*Division of Mathematics, Computer and Information Systems, Office of Naval Research, Arlington, VA 22217, USA.*

<sup>9</sup>*Department of Mechanical Engineering, University of New Mexico, Albuquerque, NM 87131, USA.*

<sup>10</sup>*Department of Computer Science, University of Milan, Milano, Italy.*

<sup>11</sup>*'Enrico Fermi' Research Center (CREF), Via Panisperna 89A, 00184 - Rome, Italy.*

<sup>12</sup>*Dipartimento di Ingegneria Civile, Informatica e delle Tecnologie Aeronautiche, Università degli Studi 'Roma Tre', Via Vito Volterra 62, 00146 - Rome, Italy.*

<sup>13</sup>*Department of Molecular Science and Nanosystems and ECLT, Ca Foscari University of Venice, Venice, 30123, Italy.*

<sup>14</sup>*London Institute for Mathematical Sciences, Royal Institution, 21 Albemarle St London W1S 4BS, UK.*

<sup>15</sup>*Research Institute of Molecular Pathology (IMP), Vienna Biocenter (VBC), Campus-Vienna-Biocenter 1, 1030 Vienna, Austria.*

30 In his book 'A Beautiful Question' <sup>1</sup>, physicist Frank Wilczek argues that symmetry is 'na-  
31 ture's deep design,' governing the behavior of the universe, from the smallest particles to the  
32 largest structures <sup>1-4</sup>. While symmetry is a cornerstone of physics, it has not yet been found  
33 widespread applicability to describe biological systems <sup>5</sup>, particularly the human brain. In  
34 this context, we study the human brain network engaged in language and explore the re-  
35 lationship between the structural connectivity (connectome or structural network) and the  
36 emergent synchronization of the mesoscopic regions of interest (functional network). We ex-  
37 plain this relationship through a different kind of symmetry than physical symmetry, derived  
38 from the categorical notion of Grothendieck fibrations <sup>6</sup>. This introduces a new understand-  
39 ing of the human brain by proposing a local symmetry theory of the connectome, which ac-  
40 counts for how the structure of the brain's network determines its coherent activity. Among  
41 the allowed patterns of structural connectivity, synchronization elicits different symmetry  
42 subsets according to the functional engagement of the brain. We show that the resting state  
43 is a particular realization of the cerebral synchronization pattern characterized by a fibra-  
44 tion symmetry that is broken <sup>7</sup> in the transition from rest to language. Our findings suggest  
45 that the brain's network symmetry at the local level determines its coherent function, and we  
46 can understand this relationship from theoretical principles.

## 47 1 Introduction

48 The network of internal connections crucially shapes collective phenomena in complex dynamical  
49 systems <sup>8</sup>. In particular, synchronization, which is a collective behavior in which the dynamics  
50 of the network nodes converge on the same time evolution, can be exhibited either as a global  
51 state <sup>9</sup> in which all units follow the same trajectory, or via clustered states where the system splits  
52 into subsets of units synchronized to each other <sup>10,11</sup>. In the latter phenomenon, known as cluster  
53 synchronization (CS) <sup>10,11</sup>, a key role in determining the composition of the clusters is played by the  
54 symmetries inherent to the network structure of connections <sup>10-19</sup>. This means that the symmetries  
55 of a network can theoretically predict the existence of CS emerging from a dynamics defined on  
56 the network.

57 Here, we find that the cluster synchronization observed in the human brain at the mesoscopic  
58 scales of regions of interest (ROIs) measured by functional magnetic resonance imaging (fMRI) is  
59 deeply intertwined with the symmetries of the brain network. These symmetries explain how the  
60 structural connections among the system's ROIs (connectome or structural network) determine the  
61 emergent dynamical synchronization expressed in the functional network in the resting state (RS)  
62 and during a cognitive task of language.

63 Relating the 'structure' to 'function' is a long-standing problem in systems science <sup>20-24</sup>. Ear-  
64 lier empirical studies of the structure-function relationship in the human brain have used diffusion  
65 tractography and fMRI to correlate white matter tracts to the functional coupling between the ROIs  
66 <sup>23,25-27</sup>. Statistical analyses have shown correlations between the structural connectivity (obtained

67 from DTI) and resting state functional connectivity (obtained from fMRI) between anatomically  
68 defined ROIs <sup>23,25–27</sup>. While the structural connectivity partially resembles the resting state func-  
69 tional connectivity; two ROIs can be structurally connected but not functionally related, and vice  
70 versa.

71 More recently, the structure-function relation has been investigated by neurodynamical mod-  
72 eling of fMRI signals in resting and task-based cognitive states <sup>28,29</sup>. These models are validated  
73 by comparing predicted spatiotemporal patterns with empirical functional connectivity data. Geo-  
74 metric constraints of curvature and distance have been shown to shape both the spontaneous and  
75 induced activity of the brain <sup>30</sup>. These latest results suggest a principled theoretical approach to  
76 understanding how structure shapes function is possible.

77 In this paper, we postulate that a symmetry theory of the connectome sheds light on how  
78 structure determines function by predicting the synchronization of the brain ROIs. We show that  
79 the theory of symmetry— and symmetry-breaking <sup>7</sup>— widely used in physics <sup>1–3</sup>, geometry <sup>31</sup>,  
80 dynamical systems <sup>10–13</sup>, and geometric deep learning <sup>32</sup>, can bridge the gap between the brain  
81 network structure and its dynamic synchronization.

82 The symmetries we find in the human brain are not those of physical systems. Physical  
83 (and geometrical) symmetries are automorphisms and form symmetry groups <sup>2,3</sup>. These are global  
84 symmetries since they preserve the global shape of objects, and, in the particular case of graphs,  
85 they are permutations of nodes that preserve the global adjacency of nodes. Instead, the sym-  
86 metries we find in the brain network are symmetry fibrations <sup>14,18</sup>— derived from Grothendieck  
87 fibrations in category theory <sup>6</sup>— which form symmetry groupoids <sup>12,13</sup>. Fibrations are less re-  
88 stricted symmetries than automorphisms because they are local symmetries that preserve only the  
89 color-isomorphic inputs of nodes. Consequently, they preserve the dynamical evolution leading to  
90 cluster synchronization in the network.

91 Fibrations have been proven to be a useful tool for describing how genetic networks are built  
92 from the bottom up to process information through gene expression <sup>12,17–19,33</sup>. They also appear  
93 in simple *C. elegans* neural circuits <sup>17,34–36</sup>, and are crucial in explaining the expressiveness and  
94 power of graph neural networks <sup>37,38</sup>.

95 Here, we expand this view to the human brain, letting the empirical activity of synchro-  
96 nization drive the inference of the underlying connectome. We implement a symmetry-driven  
97 algorithm based on a mixed integer linear programming to infer the structural network that sus-  
98 tains the cluster synchronization of the functional language network (a brain’s specific cortical  
99 sub-network involved in the language function <sup>24</sup>) obtained experimentally in different processes  
100 whose outcome is the human language ability.

101 In analogy to the theory of phase transitions between states in physical systems <sup>7,39</sup>, we

102 describe the recruiting of communication resources across different brain states as a process of  
103 network-symmetry breaking. First, we find that the baseline connectome of the language network  
104 displays a global group symmetry that switches to a local fibration symmetry to sustain the rest-  
105 ing state synchronization dynamics. Then, this symmetry is further broken by the activity-driven  
106 lateralization induced by the language task. The brain switches from the resting state to the execu-  
107 tion of language inducing a fibration symmetry breaking of the connectivity pattern sustaining the  
108 synchronization of the brain regions.

## 109 2 Cluster synchronization in the functional network

110 **2.1 Functional network of synchrony between ROIs from fMRI.** We analyze fMRI BOLD  
111 signals from  $n(= 20)$  subjects (normal, healthy volunteers with no neurological or psychiatric  
112 morbidities) at rest and while performing two language tasks to construct functional networks as-  
113 sociated with expressive language. We build functional networks as a group average over subjects  
114 performing two well-studied language tasks, phonemic fluency, and verb generation<sup>40</sup>, and at rest  
115 <sup>41</sup> (Fig. 1 and Methods Sec. 6.3). During the phonemic fluency task, the subjects are asked to  
116 silently generate as many words as possible, starting with a given letter. During the verb genera-  
117 tion task, subjects are asked to generate action words associated with the presented nouns. During  
118 the resting state, subjects are instructed to lie in the scanner with their eyes open, try to think of  
119 nothing in particular, and fixate on a central cross on a screen.

120 The functional network is built between anatomically defined ROIs that are primarily in-  
121 volved in language according to the dual stream model<sup>42,43</sup> (see Fig. 1a and Methods Sec. 7 for  
122 more details). Specifically, we consider the dorsal stream of the dual stream model in our anal-  
123 ysis: Supplementary Motor Area (SMA), Premotor Area (PreMA, left and right), Supramarginal  
124 Gyrus (SMG left and right), Broca’s Area (BA, left and right), Angular Gyrus (AG, left and right),  
125 and Wernicke’s Area (WA, left and right). Many other secondary areas of the brain are involved  
126 in language. This gets more complicated in pathological states such as brain tumors that lead to  
127 language reorganization. Here, we focus our analysis on these primary language areas and their  
128 connections.

129 We use standard methods to build the functional network from the time-dependent fMRI-  
130 measured blood-oxygen-level-dependent (BOLD) signal<sup>22</sup> (see Methods Sec. 8). For a single  
131 subject, we measure synchronization using the Phase-Locking Value (PLV)<sup>44</sup> among the BOLD  
132 time series between ROI pairs (see Extended Data Fig. 5 and Methods Sec. 9). We obtain the  
133 correlation matrix observed in Extended Data Fig. 6 for a typical subject. Averaging these matrices  
134 across  $n$  subjects, we obtain a weighted group-average correlation matrix with edge weights in the  
135  $[0, 1]$  range. Using this correlation matrix, we obtain the functional network from which the CS of  
136 ROIs are obtained.

137 Ideally, a perfect CS is a non-overlapping, fully connected induced subgraph (clique) embed-

138 ded in the functional network. Since this ideal synchronization cannot be expected from real data;  
 139 we relax this condition by allowing the fully connected subgraph to be connected by weak inter-  
 140 clique links. We define a CS  $N$ -clique as the induced, fully connected subgraph of the functional  
 141 network composed of  $N$  nodes that satisfy the following conditions:

$$\sum_{i < j}^{1, N} \sigma(x_i(t), x_j(t)) \geq \frac{N(N-1)}{2} \sigma(x_k(t), x_{k'}(t))$$

$$\forall k = 1, \dots, N \text{ and } k' \in \mathcal{M}_k, \quad (1)$$

142 where  $\mathcal{M}_k$  is the set of nearest neighbors of node  $k = 1, \dots, N$  not belonging to the considered  
 143 clique, and  $\sigma(x_i(t), x_j(t))$  is the PLV of the functional time series  $x_i(t)$  and  $x_j(t)$  of nodes  $i$  and  $j$ ,  
 144 respectively (see Extended Data Fig. 5 and Methods Sec. 9 for further details).

145 The clusters of synchronized ROIs are obtained by applying a standard percolation threshold  
 146 procedure<sup>45,46</sup> to the correlation matrix. Starting from a disconnected graph, links between nodes  
 147 are progressively added in decreasing order of weight of the correlation matrix (i.e., synchroniza-  
 148 tion), starting from the largest one. A CS clique is found as soon as the condition in Eq. (1) is  
 149 satisfied. The process stops when the weight of the links to add doesn't allow further cliques to  
 150 form. This process defines a hierarchy of CS according to the order of clique appearance in the  
 151 percolation process.

152 **2.2 Cluster synchronization in resting state and task.** The RS-CS is calculated from the func-  
 153 tional network between the ROIs defined in Sec. 2.1 and the correlation matrix built from their  
 154 fMRI signals obtained in the RS experiments (see Methods Sec. 10). The result for the group aver-  
 155 age correlation matrix is shown in Fig. 2b. Using this correlation matrix, we obtain the functional  
 156 network displayed in Fig. 2a with the synchronized clusters of ROIs from Eq. (1) is shown in  
 157 different colors. It is known that the RS functional network is approximately left-right symmetric  
 158<sup>47,48</sup>. Our results confirm this evidence by demonstrating bilateral synchronization of three CS (Fig.  
 159 2a). Each comprises a bilateral pair of regions (supramarginal gyrus, angular gyrus, and Broca).  
 160 Beyond this expected result, we find a novel central CS composed of a pentagonal clique of two  
 161 bilateral pairs of regions (premotor and Wernicke's area) and the supplementary motor area. This  
 162 CS fits the auditory-motor integration mechanism of the dorsal stream of the language processing  
 163 model (see Methods Sec. 10 for more details).

164 A different functional network is activated when the subject performs a language task. We  
 165 find that a common feature of both verb generation (Fig. 2 c and d) and phonemic fluency (Fig. 2  
 166 e and f) networks is the emergence of left lateralization<sup>24</sup> by the engagement of BR left and left  
 167 frontal language areas in the task. We find that the BA left area is recruited by SMA, becoming,  
 168 in the process, desynchronized with BA right, which, in turn, synchronizes with WA left and  
 169 right. The CS set is identical in both language tasks (Figs. 2 c and e), yet the clusters appear

170 in different orders in the CS hierarchy. During verb generation, the bilateral PreMA cluster is  
 171 more synchronized than the AG one, while things are reversed during the phonemic fluency task.  
 172 Finally, the two less synchronized clusters are the same in both tasks: the triangle composed of  
 173 the bilateral WA, the right BA, and the bilateral SMG. These results are consistent with the current  
 174 understanding of language modeling (see Methods Sec. 10).

### 175 3 Theory of global and local symmetries

176 **3.1 Automorphisms and fibration symmetries.** Once we have specified the pattern of CS  
 177 within the language functional network, we present a symmetry theory to infer the structural lan-  
 178 guage network that sustains the observed synchronization. Classically, symmetries are mathemat-  
 179 ically captured by **automorphisms**<sup>49</sup>. In a graph, an automorphism is a permutation of the nodes  
 180 of the graph that preserves the global adjacency connectivity (Fig. 3a and Methods Sec. 11). That  
 181 is, the (in-coming and out-going) neighbors of *every* node are preserved by the permutation: note  
 182 that this is a *global* condition because the map involves all nodes. The clusters of nodes subjected  
 183 to these permutations are called **orbits**, and nodes within each orbit synchronize their activity un-  
 184 der a dynamical system admissible for the network. The requirements for the existence of orbits  
 185 are hard (i.e., difficult to satisfy) and **global**, as automorphisms must preserve the entire adjacency  
 186 matrix.

187 Conversely, a graph homomorphism called **graph fibration**<sup>14,18</sup>, allows for the definition  
 188 of less constrained (i.e., more general) **local** symmetries than do automorphisms (Methods Sec.  
 189 12). Graph fibrations are derived from the categorical notion with the same name, introduced by  
 190 Grothendieck and others in the 1960’s<sup>6</sup>.

**Definition 1 (Fibration).** *Given a graph  $G = (N_G, E_G)$ , a graph fibration  $\phi$  of  $G$  to a base graph  $B = (N_B, E_B)$  is a homomorphism (Fig. 3b, right)*

$$\phi : G \rightarrow B, \tag{2}$$

191 that satisfies the following *lifting property*<sup>14</sup>:

**Definition 2 (Lifting Property).** *For any edge  $e_B \in E_B$  and any node  $n_G \in N_G$  such that  $\phi(n_G) = t(e_B)$  (where  $t$  is the function that specifies the target node of each edge), there is a unique  $e_G \in E_G$ , called the *lifting* of  $e_B$  at  $n_G$ , such that*

$$\phi(e_G) = e_B \quad \text{and} \quad t(e_G) = n_G. \tag{3}$$

192 Otherwise, a fibration is a graph homomorphism that is only required to be a bijection of  
 193 *local in-neighborhoods* rather than of the entire network. Therefore, it is truly a local symmetry  
 194 and much less constrained than the global symmetries of automorphisms.

195 An equivalent, and perhaps more intuitive, definition of graph fibration was given in <sup>18</sup> and  
196 grounds on the concept of an input tree of a graph's node (see Fig. 3b, left).

197 **Definition 3 (Input tree).** *The input tree for a node  $v$ , denoted  $T(v)$ , is a rooted tree centered*  
198 *at node  $v$ . The first layer of the tree is the node's in-neighborhood, called its input set. Each*  
199 *subsequent layer is then iteratively defined as the input set of the input set.*

200 The input tree represents the complete set of all paths that terminate on  $v$  and thus represents  
201 the dynamical history of the information flow arriving at  $v$  through the network. Accordingly, we  
202 can use the input tree to define cluster synchronization in the network.

203 A fibration  $\phi$  of  $G$  “collapses” the nodes of  $G$  with isomorphic input trees into the base  $B$ ,  
204 see Fig. 3b right. A fibration that produces the minimal base (i.e., maximum collapse) is referred to  
205 as the **symmetry fibration** of  $G$  because it collects all the symmetries of the network <sup>18</sup>. Clustered  
206 nodes with isomorphic input trees are called **fibers** (the colored nodes in Fig. 3b) and are analogous  
207 within the fibration framework to group orbits in the automorphisms world. (Note: ‘fiber’ in the  
208 context of fibration should not be confused with ‘fiber’ in the context of ‘fiber-tracks’).

209 A fundamental theoretical results proved by DeVille and Lerman <sup>15</sup> [Theorem 4.3.1 and  
210 Lemma 5.1.1] (see also <sup>12,16</sup>) has profound consequences for the structure-function relation by  
211 allowing the gap between the fibration of the graph (structure) and the existence of CS (function)  
212 to close:

213 **Definition 4 (Fiber synchrony).** *The set of nodes in the same fiber of the fibration (i.e., with*  
214 *isomorphic input trees) is proven to be synchronous under a dynamical system defined on the*  
215 *network. This result is quite general since it is independent of the type of dynamics considered, as*  
216 *long as it is admissible with the graph.*

217 The partition of nodes into fibers of a fibration coincides with the partition obtained by **bal-**  
218 **anced coloring**, or equitable partition <sup>12-14</sup>. This correspondence provides a third alternative  
219 definition of a graph fibration in terms of the input sets rather than the input trees:

220 **Definition 5 (Balanced coloring = fiber synchrony = CS).** *A balanced coloring of a graph is an*  
221 *assignment of colors to nodes, such that nodes of one color receive the same amount of the other*  
222 *colors from their in-neighbors (i.e., same number of in-neighbors of each other color, see Fig. 3b,*  
223 *right).*

224 Aldis <sup>50</sup> [Theorem 4.2 and Corollary 4.3] has indeed shown that the fibers of the fibration are  
225 the partition induced by balanced colorings of the graph. Thus, we identify the CS obtained from  
226 the dynamics with the fibers of the graph or analogously the balanced coloring.

227 The orbital partition obtained from automorphisms (Fig. 3a, right) is also a balanced coloring  
228 but is generally finer than the coarsest balanced coloring determined by the symmetry fibration:  
229 i.e., every orbit is a fiber, but not every fiber is an orbit. This implies that a graph may have more  
230 fibration symmetries than those induced by the automorphisms (Fig. 3b).

231 In other words, all automorphisms are fibrations, but not all are automorphisms. Intuitively,  
232 the conditions imposed by automorphisms, being on non-local scales, are much harder to satisfy  
233 than in vibrations, which preserve only the local in-neighborhood. Algorithms to efficiently calcu-  
234 late the minimal balanced colorings (fibers) in a network exist <sup>18,19,51</sup>. They are also widely used  
235 in machine learning and GNN as the Weisfeiler-Lehman graph isomorphism test <sup>37</sup>. Orbits and  
236 automorphisms are calculated with McKay’s Nauty algorithm <sup>52</sup>.

237 **3.2 The symmetries of the dual stream baseline connectome of language.** Having defined  
238 symmetries, we now look for them in the connectome of white-matter fiber tracks between the  
239 ROIs primarily involved in language <sup>53</sup>. The known bundles of axonal tracks between ROIs in the  
240 dorsal stream model is shown in the connectome displayed in Fig. 1a, right (see Methods Sec. 13  
241 for more details). They are those of the dorsal stream formed by white-matter tracks of the superior  
242 longitudinal fasciculus (SLF) arcuate fasciculus (AF) system. In brief, the AF connects the inferior  
243 frontal gyrus (Broca’s area) to the posterior superior temporal gyrus (Wernicke’s area). The SLF  
244 connects Broca’s area and premotor area to the inferior parietal areas (supramarginal and angular  
245 gyri) <sup>53,54</sup>. The frontal aslant tract (FAT) connects Broca’s area with the supplementary motor area,  
246 serving the verbal fluency components of language <sup>55,56</sup>. Sensorimotor integration culminates in  
247 the Broca’s area and ventral PreMA, which are responsible for articulatory planning <sup>57,58</sup>. Two  
248 parallel dorsal pathways <sup>24</sup> connects the PreMA (dorsal pathway I) and Broca (dorsal pathway  
249 II) to Wernicke in order to predominantly support sound-to-motor mapping. The second supports  
250 higher-level language processes.

251 These tracks constitute the *dual stream (dorsal) baseline connectome* of language shown in  
252 Fig. 1a. A symmetry analysis of this connectome reveals a remarkable symmetry (Fig. 4a): in such  
253 a network, the number of fibers and orbits are equal (equal to five; see Methods Sec. 14). This  
254 means that the automorphisms (symmetry group) and the fibration symmetries of this network are  
255 the same, implying that the global symmetry is the same as the local.

256 According to both orbital and fiber partitions, the five fibers (orbits) are (Extended Data fig.  
257 7): a 4-ROI cluster composed of WA (left and right) and SMG (left and right), and fibers respecting  
258 the left-right symmetry: PreMA (left and right), BA (left and right), AG (left and right), and SMA  
259 (alone).

260 For instance, the input trees of  $WA_L$ ,  $WA_R$ ,  $SMG_L$  and  $SMG_R$  are isomorphic (Extended  
261 Data Fig. 7c). Therefore, these ROIs belong to the same fiber and are collapsed by fibration  
262 symmetry. At the same time, the permutation that maps  $WA_L$  to  $SMG_L$ , and  $WA_R$  to  $SMG_R$

263 (displayed in Extended Data Fig. 7b) in cycle notation:  $\pi_2 = (WA_L SMG_L)(WA_R SMG_R)$  is  
264 also an automorphism marking the presence of the global permutational symmetry. This creates  
265 the fiber (= orbit) colored red in Fig. 4a. This fibration=automorphism situation is a condition  
266 of high symmetry. It means an intrinsically highly symmetric network represents the highway of  
267 inter-regional communicability that allows language processing to emerge.

268 Given this initial baseline symmetric connectome, a stable pattern of synchronization can  
269 emerge during a functional engagement (Fig. 2) that should induce a modification of the symme-  
270 tries needed to sustain each functional synchronization. Hence, breaking this high initial symmetry  
271 is expected to be a crucial condition for effective functional activity. Lower symmetric states are  
272 expected when the orbits are more than the fiber (indicating a loss of global group symmetry) or  
273 when the number of fibers increases, indicating a loss (breaking) of local fibration symmetry. We  
274 explore these cases next.

275 **3.3 Inferring the structural network sustaining RS and language from cluster synchroniza-**  
276 **tion.** The baseline connectome represents the set of available routes composing the primary in-  
277 formation highway of the brain involved in language. However, which routes of this highway are  
278 utilized depends on the type of task to which the brain responds<sup>20</sup>. The main hypothesis postulated  
279 in<sup>20</sup> is that the brain’s functional activity utilizes a subset of the links available in the ‘highway’  
280 connectome to operate in each functional state. This ‘one-to-many’ degenerate structure-function  
281 relation<sup>20</sup> allows the emergence of diverse functional states (resting, language, etc.) from a unique  
282 static connectome architecture. In the present case, it means that, given the dorsal stream baseline  
283 connectome in Fig. 1a, different subsets of this connectome mediate different functional networks  
284<sup>20,21</sup>. We demonstrate this structure-function relation by matching the patterns of ROI synchro-  
285 nization and coloring clustering obtained from Fig. 2 to different realizations of the structural  
286 network.

287 Accordingly, we infer the structural network associated with each balanced coloring of the  
288 functional network obtained experimentally in RS and task. To this end, we develop a mixed  
289 integer linear programming (MILP)<sup>35,59</sup> algorithm to optimize a minimal link removal from the  
290 connectome to satisfy the balanced coloring obtained in the experiments. The ‘one-to-many’ hy-  
291 pothesis is falsifiable. If true, MILP must find a solution to the color partitioning using only  
292 removals. If there is no solution, then the hypothesis is wrong.

293 The inference algorithm can be summarized in the following steps (Fig. 1 and Methods Sec.  
294 15):

- 295 • For a given set of ROIs (Fig. 1a left), identify the baseline connectome that form the graph  
296 of all permitted structural connections among them (Fig. 1a right);
- 297 • Using the PLV synchronization measure, find the CS from the functional network according

298 to Eq. (1) for a given task (Fig. 2a, c, e). Assign to each ROI in each CS in the functional  
299 network a color symbolizing the fiber partition or balanced coloring.

- 300 • Decimate the baseline connectome by removing the minimal number of edges until the fibers  
301 of the decimated graph match the coloring obtained from the functional network (Fig. 1b  
302 right).

303 We apply this algorithm to identify the routes that sustain the functional network at rest and  
304 during the execution of the two language tasks. Although the ranking of the CS is different for  
305 the two tasks, the coloring is not. It means the structural network that sustains the two types of  
306 functional activity in language is the same.

#### 307 4 Symmetry-breaking transition to resting state and task

308 While symmetry principles stand as crucial elements within natural laws, much of the world's  
309 complexity emerges from mechanisms of symmetry breaking, which encompasses various ways  
310 nature's symmetry can be veiled or disrupted<sup>7,39</sup> (Methods Sec. 16). Any situation in physics in  
311 which the ground state (i.e., the state of minimum energy) of a system has less symmetry than the  
312 system itself, exhibits the phenomenon of spontaneous symmetry-breaking. For instance, different  
313 phases of matter are characterized by different symmetries. At higher temperatures, matter takes on  
314 a 'higher symmetry' phase (e.g., paramagnetism, normal conductivity, and fluidity), while at lower  
315 temperatures, the symmetries of the phases are broken to 'lower symmetry' (e.g., ferromagnetism,  
316 superconductivity, and superfluidity).

317 Although the connectome is not a dynamic state per se, we can explain the transitions from  
318 the baseline highway of connections to its subset responsible for sustaining the communication  
319 processes at rest and task analogous to symmetry breaking in ferromagnets. Starting from the  
320 baseline connectome with high symmetry configuration as estimated by orbits and fibers (Fig. 4a),  
321 we find progressive and different symmetry-breaking processes in the structural connectivity as the  
322 brain engages in different states (Fig. 4b and c).

323 The first symmetry-breaking transition occurs once the dynamics are introduced. Figure 4b  
324 shows the balanced coloring of the inferred structural network sustaining the resting state synchro-  
325 nization. A symmetry analysis of this network (see Methods Sec. 17 and Extended Data Fig. 8)  
326 shows that while in the baseline connectome, we have both fibrations and automorphisms, in the  
327 resting state condition, the group symmetry, including the global left-right symmetry, is lost, and  
328 the fibration symmetry is enhanced. We find four fibers in the resting state (four colors in Fig. 4b)  
329 vs. five fibers found in the baseline connectome (Fig. 4a).

330 When synchronization processes intervene, the symmetry is broken in the precise direction  
331 of the optimal communicability among the brain regions. The resting state dynamics introduce

332 a mismatch between orbits and fibers. Fibration symmetry increases (fewer fibers) during the  
333 resting state synchronization (Extended Data Fig. 8a left and 8c), while a total loss of group  
334 symmetry is produced (Extended Data Fig. 8a right and 8b). Remarkably, while the global left-  
335 right symmetry is disrupted in the RS connectome, the local left-right fibration symmetry necessary  
336 for left-right synchronization is still maintained. This suggests that the perturbation represented  
337 by brain synchronization on the static network neutralizes the automorphism, but reinforces the  
338 biological fibration configuration, which in turn allows the stability of the synchronized dynamics.

339 Figure 4c shows the balanced coloring of the inferred structural network engaged in the lan-  
340 guage (see symmetry analysis in Methods Sec. 18 and Extended Data Fig. 9). During the execution  
341 of the task, the activity is largely polarized in recruiting areas devoted to the correct functioning.  
342 The lateralization of brain activity during language execution induces a further fibration symmetry-  
343 breaking between the Broca left and Broca right areas, which now belong to two different fibers as  
344 seen in Fig. 4c. Broca left is recruited by the SMA, while Broca right is recruited by the Wernicke  
345 pairs, which remain locally symmetric. The number of fibers is increased to five (less symmetry)  
346 compared to the fibration symmetry in RS, as if the activity induced by the task execution acts as  
347 a perturbation over the resting state dynamics. The global symmetry remains completely broken,  
348 presenting only the trivial (identity) automorphism, and one orbit per ROI (Extended Data Fig. 9a  
349 right and 9b).

350 The five fibers found and the lateralization characterizing them are compatible with the  
351 neurocognitive models of the functional circuits of language production. Indeed, studies have  
352 demonstrated that networks involving the temporal cortex and the inferior frontal cortex, predom-  
353 inantly lateralized to the left hemisphere, are implicated in supporting syntactic processes, while  
354 temporo-frontal networks with less lateralization are involved in semantic processes<sup>60,61</sup>. Thus,  
355 the symmetry-breaking is found to be a direct consequence of cognitive specialization of brain  
356 areas (specifically the group SMA, BA, and WA), for the elaboration of specific tasks (i.e., syn-  
357 tactic tasks) as it happens also to other regions of the brain that give place to a recognized brain  
358 asymmetry<sup>62</sup>.

359 The description of the brain region's recruitment during a task execution as a symmetry-  
360 breaking process is only possible because the pattern of connections that support the communica-  
361 tion among such regions change selectively according to the specific conditions in which the brain  
362 is. Different dynamics can be matched with different patterns of structural connectivity unveiled  
363 by symmetry considerations. As a consequence, the mesoscopic matching of the brain's structural-  
364 to-functional connectivity emerges as a reconfiguration process driven by the fibration symmetry  
365 induced by the communication dynamics among brain regions.

## 366 5 Discussion

367 We propose a symmetry theory of brain connectivity whose possible functional transitions can  
368 be pooled in determined sets of breaking symmetry processes. The primary application of the  
369 synchronization-driven inference method proposed here is the understanding of disease pathways.  
370 The inference of pathways from dynamical data on healthy subjects can be extended to neurolog-  
371 ical or psychiatric conditions, allowing the identification of differential disease pathways, leading  
372 to an understanding of the disease, establishing the diagnosis, and ameliorating the consequences.  
373 Moreover, our method can be beneficial for drug development by targeting the inferred structural  
374 network of a specific disease onto a healthy one. Finally, the controllability of brain networks,  
375 which is an open problem in neuroscience should find a boost from the results reported here.  
376 The treatment of neurological and psychiatric diseases through invasive (surgery) or non-invasive  
377 (electric/magnetic stimulation) intervention <sup>40</sup> will benefit from the identification of the patterns of  
378 symmetry and synchronization and their breaking processes to reduce side effects or to optimize  
379 the effectiveness of the application.

380 Overall, our findings suggest that the brain's local symmetry at the mesoscopic level de-  
381 termines its coherent function. Symmetry fibrations strictly generalize the symmetry groups of  
382 physics and have been found in biological systems from the human brain and *C. elegans* connec-  
383 tome to genetic and metabolic networks. Thus, if symmetry fibrations can be postulated to be  
384 'nature's deep design', they will unify not only physics but also biology, providing a plausible  
385 solution to the aforementioned conundrum.

## 386 Methods

### 387 6 Experimental protocols

388 **6.1 Subjects.** Twenty healthy right-handed subjects (mean age= 37, SD=12; 7 females and 13  
389 males) without any neurological history participated in the study. The study was approved by the  
390 Institutional Review Board at Memorial Sloan Kettering Cancer Center, in compliance with the  
391 declaration of Helsinki and informed consent was obtained from each subject.

392 **6.2 MRI methods.** A GE 3T scanner (General Electric, Milwaukee, Wisconsin, USA) and a  
393 standard quadrature head coil was employed to acquire the MR images. Functional images cov-  
394 ering the whole brain were acquired using a (T2\*)-weighted imaging sequence sensitive to blood  
395 oxygen level-dependent (BOLD) signal (repetition time, TR/TE = 2500/40 ms; slice thickness =  
396 4.5 mm; matrix = 128 × 128; FOV = 240 mm; volumes = 160). Functional matching axial T1-  
397 weighted images (TR/TE = 600/8 ms; slice thickness = 4.5 mm) were acquired for anatomical  
398 co-registration purposes.

399 **6.3 Language tasks and RS.** All subjects performed a resting-state task, a verbal fluency task  
400 using verb generation in response to auditory nouns and a phonemic fluency letter task in response  
401 to task instructions delivered visually.

402 During the resting state condition, subjects are asked to lie in the scanner and to keep their  
403 eyes open, to try to think of nothing in particular, and to keep fixating on a central cross on a screen  
404 during the RS.

405 In the verb generation task, subjects were presented with a noun by oral instruction and then  
406 asked to generate verbs associated with the noun. For example, subjects are presented with a noun  
407 (e.g., 'baby') and asked to generate verbs (e.g., 'cry,' 'crawl') associated with the noun. Subjects  
408 perform the task silently to avoid motion artifacts. Four nouns are displayed over eight stimulation  
409 epochs, each lasting 50 s, allowing 32 distinct nouns to be read over the entire duration. Each  
410 epoch consisted of a resting period (30 s) and a task period (20 s).

411 In the phonemic fluency task, on the other hand, subjects are asked to generate nouns that  
412 begin with a given letter silently. For instance, the subject presented with the letter 'A' may generate  
413 words such as 'apple,' 'apron,' or 'ashtray.' Stimuli are displayed on a screen over eight stimulation  
414 epochs, each lasting 20 s. During the task, two letters are presented in each stimulation epoch. Each  
415 epoch also consisted of a 30-second resting period during which subjects were asked to focus on a  
416 blinking crosshair.

417 In order to avoid artifacts from jaw movements, subjects were asked to silently generate the  
418 words.

419 **6.4 Data preprocessing.** Functional MRI data were processed and analyzed using the software  
420 program Analysis of Functional NeuroImages (AFNI; Cox, 1996). Head motion correction was

421 performed using 3D rigid-body registration. The first volume was selected to register all other vol-  
422 umes. The first volume was chosen because it was acquired before the anatomical scan. During the  
423 registration, the motion profile was saved and regressed. Spatial smoothing was applied to improve  
424 the signal-to-noise ratio using a Gaussian filter with a 4 mm full width of half maximum. Correc-  
425 tions for linear trend and high-frequency noise were also applied. Resting-state data requested  
426 some more preprocessing steps. They were corrected for head motion by regressing head motion  
427 data and the first five principal components of the white matter and CSF signals. They were also  
428 detrended, demeaned, and band-pass filtered (frequency range 0.01-0.1 Hz). All fMRI data were  
429 registered to the standard space (Montreal Neurological Institute MNI152 standard map). Task  
430 data for task state synchronization analyses were additionally preprocessed using a general linear  
431 model. The stimulation scheme was removed by fitting the task timing (block design) for each  
432 condition. This was accomplished using the convolution of the block design with a standard 2-  
433 gamma hemodynamic response function used for the task activation estimates, fit simultaneously  
434 with its derivative.

## 435 **7 Definition of ROIs: dorsal stream model of language**

436 The modeling of language processing has been based for a long time on the Geschwind-Lichteim-  
437 Wernicke model<sup>63</sup>, primarily drawn from observations of individuals with brain injuries. Fol-  
438 lowing this model, words are perceived through a dedicated word reception center (Wernicke's  
439 area) within the left temporoparietal junction. Subsequently, this region sends signals to a word  
440 production center (Broca's area) in the left inferior frontal gyrus.

441 Advancements in electrophysiological and MRI techniques have unveiled a dual auditory  
442 pathway. This led to the development of a dual stream model<sup>42,43</sup>. According to this model, two  
443 distinct pathways connect the auditory cortex to the frontal lobe, each serving different linguistic  
444 functions. The auditory ventral stream pathway is responsible for sound recognition and is called  
445 the auditory 'what' pathway. On the other hand, the auditory dorsal stream, found in humans and  
446 non-human primates, is responsible for sound localization and is called the auditory 'where' path-  
447 way. In humans, particularly in the left hemisphere, this pathway also handles speech production,  
448 repetition, lip-reading, phonological working memory, and long-term memory.

449 The relevant ROIs are those areas involved in the two language tasks considered. Since the  
450 tasks are both focused on language production (phonemic fluency and verb generation), regions of  
451 the dorsal stream are part of the analysis (Fig. 1): Supplementary Motor Area (SMA), Premotor  
452 Area (PreMA, left and right), Supramarginal Gyrus (SMG left and right), Broca's Area (BA, left  
453 and right), Angular Gyrus (AG, left and right), Wernicke's Area (WA, left and right). The BA and  
454 WA are recognized as responsible for language expression and comprehension. The supplementary  
455 motor area (SMA) has been largely considered involved in controlling speech-motor functions, and  
456 it has also been shown<sup>64</sup> that the SMA performs several higher-level control tasks during speech  
457 communication and language comprehension. The AG is assumed to be a region of the brain  
458 associated with complex language functions (i.e., reading, writing, and interpretation of what is  
459 written). In contrast, the SMG is involved in the phonological processing of high-cognitive tasks.

460 Finally, processing an action verb depends in part on activity in a motor region that contributes  
461 to planning and executing the action named by the verb. The premotor cortex is known to be  
462 functionally involved in understanding action language <sup>65</sup>.

## 463 **8 Structural and functional network**

464 We distinguish between the ‘structural network’ and ‘functional networks’ of the brain <sup>20,22,23</sup>.  
465 The ‘structural network,’ also called ‘connectome’ or ‘structural graph’, is a set of nodes and  
466 edges that form the brain’s underlying network of physical connections. We study the brain graph  
467 at mesoscopic scales where nodes are ROIs defined at the mm scale (measured by fMRI in the  
468 human brain) and edges are the white matter tracks that connect the ROIs. These edges are usually  
469 measured by diffusion tensor imaging (DTI) or are known from the literature. By structure, we  
470 mean the structure of this graph.

471 When a graph is equipped with state variables and dynamical equations, it technically be-  
472 comes a ‘network system’ of ODEs. Specific features of the dynamics, such as the quantitative  
473 value of interaction constants or the frequency of an oscillation, depend on the precise details of  
474 the model equations. Here, we focus on more general features, which can occur for broad classes  
475 of models and systems. Synchronization is the prime example of such a feature. We associate  
476 ‘function’ with the synchronization of ROIs measured from fMRI indicating that the ROIs are  
477 functionally related. This synchronization occurs in clusters of ROIs or CS <sup>10-13</sup>. The ‘functional  
478 network’ from where CS is obtained is built from the synchronization between ROI activity in the  
479 brain as measured by fMRI. <sup>20,21</sup>.

## 480 **9 Cluster synchronization and the functional network**

481 BOLD time series were extracted from all voxels in a sphere of radius 6 mm centered on target  
482 MNI152 coordinates addressing a ROI. Each ROI was composed of 123 voxels. The synchroniza-  
483 tion between pairs of nodes of the language network was estimated as the Phase Locking Value  
484 (PLV) <sup>66</sup> between the BOLD time series from pairs of ROIs. Once time series were obtained for  
485 the eleven ROIs included in the study (by spatial averaging the BOLD signal within each ROI at  
486 each time point), the synchronization was calculated as follows. Given the BOLD signals  $n_u(t)$   
487 and  $n_v(t)$  coming from regions  $u, v = 1, \dots, N$  ( $N = 11$ ), their instantaneous phases  $\phi_{n_u}(t)$  and  
488  $\phi_{n_v}(t)$  can be obtained by means of their Hilbert transform (see Extended Data Fig. 5). The PLV  
489  $\sigma(\phi_{n_u}(t), \phi_{n_v}(t))$  is then given by:

$$\sigma(\phi_{n_u}(t), \phi_{n_v}(t)) = |\langle e^{-j(\phi_{n_u}(t) - \phi_{n_v}(t))} \rangle_t|, \quad (4)$$

490 where  $j$  is the imaginary unit.

491 To test the statistical significance of the PLVs, a non-parametric permutation test was run  
492 by generating surrogate ROI signals randomly re-arranged and eventually time-reversed (1,000

493 permutations). This procedure allowed the generation of a null distribution that shared the same  
494 parameters (mean and standard deviation) of the original data and similar (but not identical) tempo-  
495 ral dynamics. This produced a null distribution of t-statistics that provided the one-tailed P value.  
496 P values were estimated using a generalized Pareto distribution to the tail of the permutation dis-  
497 tribution<sup>67</sup>. Correction for multiple comparisons was provided by thresholding statistical maps at  
498 the 95th percentile ( $P < 0.05$ , FDR) of the maximum t distribution from the permutation<sup>68</sup>.

499 The PLVs were then entered in a  $N \times N$  correlation matrix, representing the correlation/synchronization  
500 or PLV matrix. Finally, the PLV matrices were averaged across subjects in each experimental con-  
501 dition (resting state, phonemic fluency task, verb generation task). The functional network is then  
502 obtained by thresholding the group-averaged correlation matrix, obtaining the CS as explained in  
503 the main text.

504 The Cluster PLV shown in Figs. 2a, c, and e is the value of the weight of each link within a  
505 CS, and it is calculated as the average PLV across the edges composing the CS clique. This Cluster  
506 PLV represents the strength of the synchronization within each CS and defines the hierarchy of CS  
507 according to its strength.

## 508 **10 Cluster synchronization in resting state and tasks**

509 The patterns of CS found within the language network allow discriminating the resting state con-  
510 dition from the task ones. RS-fMRI demonstrates sub-optimal characterization of both language  
511 dominance and lateralization of eloquent areas<sup>47</sup>, due to enhance homotopic synchronization.  
512 This is especially true in networks with left-right symmetry, such as those involved in motor and  
513 vision, as well as in language, which is normally lateralized (breaking the left-right symmetry)  
514 during the execution of the task<sup>48</sup>. Our results confirm this evidence by demonstrating high left-  
515 right symmetry of the language network during resting-state. We find, according to a descendent  
516 synchronization hierarchy, a CS composed of bilateral SMG, a CS composed of bilateral BA, a  
517 pentagonal CS composed of two bilateral pairs of regions (PreMA and WA) and the SMA, and a  
518 CS composed of bilateral AG (Fig. 2 a).

519 The clusters that we find in RS are hierarchically ordered according to the Cluster PLVs as  
520 follows (Fig. 2 a and b) : the pair {SMG L, SMG R}, [PLV = 0.762], the pentagon {PreMA L,  
521 PreMA R, SMA, WA L, WA R}, [PLV = 0.712] the pair {AG L, AG R} [PLV = 0.689] and the pair  
522 {BA L, BA R}. [PLV = 0.689]. The inter-cliques connections were characterized by PLV values  
523 smaller than the Cluster PLVs: (AG R, WA R) with [PLV = 0.682], (BA L, SMA) with [PLV =  
524 0.662] and (SMG R, PreMA L) with [PLV = 0.639].

525 The large pentagonal synchronization clique composed of SMA, PreMA (bilateral), and WA  
526 (bilateral) fits the auditory-motor integration mechanism of the dorsal stream of the language pro-  
527 cessing model. As a consequence of the internal forward model, the pentagon can act as a motor  
528 speech unit that, once activated, predicts auditory consequences that can be checked against the  
529 auditory target. If they match, that unit will continue to be activated, resulting in an articulation

530 that will hit the target. If there is a mismatch, a correction signal can be generated to activate the  
 531 correct motor unit. The predictions are assumed to be generated by an internal model that receives  
 532 efferences copies of motor commands and integrates them with information about the current state  
 533 of the system and experience (learning) of the relation between particular motor commands and  
 534 their sensory consequences<sup>69</sup>. The resting state pentagonal synchronization clique enhances the  
 535 preparatory configuration for the auditory-motor integration to efficiently run when single regions  
 536 are engaged.

537 The RS functional network undergoes changes when a task is performed. The phonemic  
 538 fluency task (Fig. 2 c and d) and the verbs generation task (Fig. 2 e and f) returned very similar  
 539 patterns of synchronization, both showing the clique formed by SMA and BA L as the most syn-  
 540 chronized ones [PLV = 0.725 and PLV = 0.764 respectively]. Subsequently, the PLV hierarchy of  
 541 the cliques changes according to the task executed. The second most synchronized cliques were  
 542 (PreMA L, PreMA R) for the verbs generation task [PLV = 0.625] and (AG L, AG R) for the  
 543 phonemic fluency task [PLV = 0.699]. As opposed to the second most synchronized cliques case,  
 544 an inversion is shown, being (AG L, AG R) the third most synchronized clique for the verbs gener-  
 545 ation task [PLV = 0.624] and (PreMA L, PreMA R) for the phonemic fluency task [PLV = 0.595].  
 546 The second less synchronized clique was [WA L, WA R, BA R) both for the verb generation [PLV  
 547 = 0.560] and phonemic fluency [PLV = 0.570] tasks. Finally, for both tasks, the clique (SMG L,  
 548 SMG R) was the less synchronized one [PLV = 0.538 and PLV = 0.550 for verb generation and  
 549 phonemic fluency tasks, respectively].

550 Covert phonemic fluency tasks require phonologic access, verbal working memory, and lexi-  
 551 cal search activity, which grant a strong activation and lateralization of frontal areas<sup>70,71</sup>. Sentence  
 552 completion, such as verb generation, tasks require word recognition and comprehension, under-  
 553 standing of syntactic–semantic relationships between words, planning of a sentence structure and  
 554 word retrieval<sup>70</sup>. This leads to increased recruitment of temporoparietal language-related areas,  
 555 including WA, SMG, and AG<sup>70,72</sup>.

## 556 11 Definition of automorphisms and group symmetries

557 Basic graph theoretical definitions<sup>49</sup>:

558 **Definition 6 (Graph).** A graph  $G = (N_G, E_G)$  is defined by a set  $N_G$  of nodes and a set  $E_G$  of  
 559 arcs, endowed with two functions  $s, t : E_G \rightarrow N_G$  that associate a source and target node with  
 560 each edge.

561 **Definition 7 (Permutation of a graph).** . A permutation  $\pi$  of a graph  $G(N_G, E_G)$  is a bijec-  
 562 tive map from the set of nodes  $N_G = \{1, \dots, N\}$  to itself,  $\pi : N_G \rightarrow N_G$ , that represents the  
 563 permutation of the node labels.

564 For example, the permutation  $\pi$  in the graph of the dual stream baseline connectome in Fig.  
 565 1a that maps  $BA_L$  to  $BA_R$  while leaving all the other nodes alone is denoted in cycle notation:

$$\pi = (\text{BA}_L \text{BA}_R), \quad (5)$$

566 meaning that  $\text{BA}_L \rightarrow \text{BA}_R \rightarrow \text{BA}_L$ .

567 **Definition 8 (Permutation matrix).** A permutation matrix  $P$  is an  $N \times N$  matrix that is obtained  
568 from the identity matrix by permuting both rows and columns according to  $\pi$ .

569 For a graph with  $N$  nodes, there are  $N!$  permutations, some of which are permutation sym-  
570 metries or automorphisms, and the rest are not. The set of all permutations of the nodes of a graph  
571  $G(N_G, E_G)$  forms a group  $\mathfrak{S}_N = \{P_1, \dots, P_K\}$  where  $K = N!$ . It is called the *symmetric group* (not  
572 to be confused with a symmetry group). This set forms a group because the permutations satisfy  
573 the associative property, composition (composing two permutations leads to another permutation),  
574 and have an identity and inverse.

575 Basic group theoretical definitions <sup>73</sup>:

576 **Definition 9 (Graph homomorphism).** A graph homomorphism  $\varphi : G \rightarrow H$  (from a graph  $G$  to  
577 a graph  $H$ ) is a pair of functions  $\varphi_N : N_G \rightarrow N_H$  and  $\varphi_E : E_G \rightarrow E_H$  such that  $s(\varphi_E(a)) =$   
578  $\varphi_N(s(a))$  and  $t(\varphi_E(a)) = \varphi_N(t(a))$  for every edge  $a \in E_G$ .

579 **Definition 10 (Graph isomorphism).** A graph isomorphism  $\varphi : G \rightarrow H$  is a graph homomor-  
580 phism whose components  $\varphi_N$  and  $\varphi_E$  are both bijections.

581 **Definition 11 (Graph Automorphism).** A (graph) automorphism (also called a *symmetry permu-*  
582 *tation* or *group symmetry*)  $\pi : G \rightarrow G$  is an isomorphism from a graph to itself.

583 Alternatively, an automorphism is a permutation  $\pi : G \rightarrow G$  of the vertex set  $E_G$ , such that  
584 the pair of vertices  $i$  and  $j$  forms an edge  $(i, j)$  if and only if  $(\pi(i), \pi(j))$  also forms a edge.

585 That is, an automorphism preserves adjacency and non-adjacency of all the nodes in the  
586 graph, and therefore, it is a global symmetry: two edges are adjacent after the permutation if and  
587 only if they were adjacent before the permutation.

Any permutation matrix of a permutation  $\pi$  transforms the adjacency matrix into another  $A'$   
as  $A' = PAP^{-1}$ . If  $P$  represents an automorphism, then  $A' = A$ , and

$$A = PAP^{-1}. \quad (6)$$

588 Since the group consists of matrices, we can state this condition differently. Equation (6)  
589 holds if and only if the matrix  $P$  commutes with  $A$ , so  $PA = AP$ . Equivalently, the commutator  
590 is zero:

$$[P, A] = PA - AP = \mathbf{0}. \quad (7)$$

**Definition 12 (Symmetry group).** *Graph automorphisms form a group with respect to function composition; this group is denoted by  $\text{Aut}(G)$ :*

$$\text{Aut}(G) = \{\pi \mid \pi \text{ is a symmetry permutation of } G\}. \quad (8)$$

591 The group  $\text{Aut}(G)$  acts on the set  $N_G$ , mapping the pair  $(\pi, x) \in \text{Aut}(G) \times N_G$  to  $\pi(x) \in$   
 592  $N_G$ . The order of a finite group is the number of its elements. The generators of the symmetry  
 593 group are a subset of the group set such that every element of the group can be expressed as a  
 594 composition of finitely many elements of the subset and their inverses.

595 The set of graph automorphisms permutes certain subsets of nodes among each other. When  
 596 the symmetry group  $\text{Aut}(G)$  acts on the network, a given node  $i$  is moved by the permutations of  
 597 the group to various other nodes  $j$ . In the language of group theory, the set of all nodes to which  $i$   
 598 can be moved defines the *orbit* of node  $i$ , which in turn defines the orbital partition of the network.

**Definition 13 (Orbit of a node).** *The orbit of a node  $i \in N_G$  for the symmetry group  $\text{Aut}(G)$  is:*

$$\mathcal{S}(i) = \{j \in N_G \mid \exists \pi \in \text{Aut}(G) \text{ s.t. } \pi(i) = j\}. \quad (9)$$

599

600 It can easily be proved that two orbits  $\mathcal{S}(i)$  and  $\mathcal{S}(j)$  are equal or disjoint, and the union of  
 601 all orbits equals  $N_G$ . Therefore, the set of all orbits induces a partition of the nodes into mutually  
 602 disjoint clusters. This set of all orbits forms the *orbital partition*. The same definition can be  
 603 applied to subgroups  $H$  of  $\text{Aut}(G)$  to obtain  $H$ -orbital partitions. When  $H = \text{Aut}(G)$ , we obtain  
 604 the partition into the fewest subsets.

605 The orbital partition of the symmetry group corresponds to clusters of nodes that synchronize  
 606 under a suitable dynamical system of equations that is admissible to the graph. In other words, the  
 607 orbits guarantee that the cluster synchronization subspace is flow-invariant <sup>10,12</sup>.

608 The orbits of the symmetry group (i.e., the partition of  $N_G$  into orbital equivalence classes,  
 609 where  $x$  is equivalent to  $y$  if and only if  $\pi(x) = y$  for some automorphism  $\pi$ ) define the automor-  
 610 phism symmetry of  $G$ .

## 611 12 Definition of fibration symmetries

612 **Definition 14 (Graph Fibration).** *A homomorphism  $\phi : G \rightarrow B$  is a fibration if and only if for*  
 613 *every  $a \in E_B$  and every  $x \in N_G$  such that  $\phi(x) = t(a)$ , there exists exactly one  $a' \in E_G$  such that*  
 614  *$t(a') = x$  and  $\phi(a') = a$ . This unique arc  $a'$  is called the lifting of  $a$  at  $x$  <sup>14</sup>.*

615 **Definition 15 (Fibers of the Fibration).** *The fibers of  $\phi$  are the sets of nodes of  $G$  that are mapped*  
 616 *to the same node of  $B$ : these sets form the fiber partition of  $N_G$ .*

617 **Definition 16 (Input tree of a node).** Given a graph  $G$  and a node  $x \in N_G$  the input tree of  $x$  in  
618  $G$ ,  $T_G(x)$ , is defined recursively as follows: it is a (typically, infinite) rooted tree whose root has as  
619 many children as there are in-neighbors of  $x$  in  $G$ , and such that the subtrees rooted at each child  
620 is the input tree of the corresponding in-neighbor in  $G$ .

621 It is easy to see that if  $x, y$  are two nodes of  $G$  that are in the same fiber of *some* fibration,  
622 then  $T_G(x)$  and  $T_G(y)$  are isomorphic trees.

623 **Definition 17 (Symmetry Fibration).** For every graph  $G$ , there exists a (base) graph  $B$  and a  
624 surjective fibration  $\mu : G \rightarrow B$  such that two nodes are in the same fiber of  $\mu$  if and only if  $T_G(x)$   
625 and  $T_G(y)$  are isomorphic. This surjective fibration is essentially unique<sup>14</sup>. It collects all the  
626 symmetries of the graph and produces the (minimal) base with the minimal number of fibers: it is  
627 called the symmetry fibration<sup>18</sup>, and its fibers define the fibration symmetry of  $G$ .

**Definition 18 (Cluster synchronization (CS) in a fiber).** Cluster synchronization occurs for all  
nodes in a fiber, and they have the same dynamic state as node  $i$ , i.e.,

$$x_i(t) = x_j(t) \quad \text{if } j \in \text{Fiber}(i), \quad (10)$$

628 Such a cluster is nontrivial only for fibers of size  $> 1$ .

629 **Definition 19 (Minimal base of the symmetry fibration).** Collapsing the nodes in each fiber of  
630 the minimal fiber partition to form a single node and respecting the lifting property provides the  
631 minimal base of the symmetry fibration.

### 632 **13 Definition of the dual (dorsal) stream baseline connectome of language**

633 According to the dual stream model introduced in Methods Sec. 7, it is known that human language  
634 relies on two primary white-matter pathways: the dorsal stream, which is related to sensorimotor  
635 integration, and the ventral stream, which is related to speech comprehension<sup>53</sup>. The tracts we are  
636 interested in are the primary tracks of the dorsal stream, which is formed by white matter tracks  
637 of the superior longitudinal fasciculus (SLF) arcuate fasciculus (AF) system. The AF connects the  
638 inferior frontal gyrus (BA) to the posterior superior temporal gyrus (WA); the SLF connects BA and  
639 PreMA to the inferior parietal areas (SMG and AG)<sup>53,54</sup>. The frontal aslant tract (FAT) connects  
640 BA with the SMA, serving the verbal fluency components of language<sup>55</sup>. Sensorimotor integration  
641 culminates in the BA and ventral PreMA, which are responsible for articulatory planning<sup>58</sup>. Two  
642 parallel dorsal pathways have also been described<sup>24</sup>. One connects the PreMA (dorsal pathway  
643 I) and BA (dorsal pathway II) to the WA, with the first predominantly supporting sound-to-motor  
644 mapping and the second supporting higher-level language processes. It is also known that PreMA  
645 represents a crucial speech production hub thanks to its coupling with the SLF. Preservation of  
646 this cortical-subcortical connection is crucial for speech integrity and represents an anatomical  
647 constraint to cortical plasticity<sup>74</sup>. Additionally, homologous right- and left-sided cortical areas are

648 likely connected by the corpus callosum, the main inter-hemispheric commissure, which enables  
 649 communication between the two cerebral hemispheres <sup>75</sup>.

650 These tracks constitute the primary dual-stream baseline connectome: the set of routes com-  
 651 posing the information transfer highway within the language network. They are displayed in Fig.  
 652 1a and show a highly symmetric structure since the automorphisms are the same as the symmetry  
 653 fibrations as seen in Fig. 4a.

#### 654 **14 Analysis of symmetries of the dorsal stream baseline connectome**

655 We perform a full symmetry analysis (including group and fibration symmetry) of the dorsal stream  
 656 baseline connectome in Fig. 7.

657 McKay’s Nauty algorithm <sup>52</sup> is used to calculate the automorphisms of the connectome. The  
 658 connectome contains  $11! = 39,916,800$  possible permutations of its 11 ROIs. From this, only a few  
 659 are permutation symmetries. There are eight generators of the symmetry group of this connectome:

$$Aut(G) = \{\pi_j | \pi_j \text{ is a symmetry permutation with } j = 0, 2\}, \quad (11)$$

660 where the automorphisms (including the identity) in cycle notation are (Fig. 7b):

$$\begin{aligned} \pi_0 &= \text{Id} \\ \pi_1 &= (\text{PreMA}_L \text{PreMA}_R) (\text{BA}_L \text{BA}_R) (\text{AG}_L \text{AG}_R) \\ &\quad (\text{WA}_L \text{WA}_R) (\text{SMG}_L \text{SMG}_R) \\ \pi_2 &= (\text{WA}_L \text{SMG}_L) (\text{WA}_R \text{SMG}_R) \end{aligned}$$

661 The actions of this symmetry group generate five orbits, which is the orbital color partition  
 662 that we see in Fig. 4a and in Fig. 7a:

$$\begin{aligned} \mathcal{S}_1 &= \{\text{PreMA}_L, \text{PreMA}_R\} \\ \mathcal{S}_2 &= \{\text{BA}_L, \text{BA}_R\} \\ \mathcal{S}_3 &= \{\text{AG}_L, \text{AG}_R\} \\ \mathcal{S}_4 &= \{\text{WA}_L, \text{WA}_R, \text{SMG}_L, \text{SMG}_R\} \\ \mathcal{S}_5 &= \{\text{SMA}\} \end{aligned}$$

663 The fibration analysis is done by searching for the minimal balanced coloring of the network  
 664 using the refinement algorithm of Kamei and Cock <sup>51</sup> employed by Morone *et al.* in <sup>18</sup>. The

665 minimal balanced coloring of the graph corresponds to a balanced coloring with a minimal number  
 666 of colors. Each cluster of balanced coloring is a fiber. The resulting coloring is shown in Fig. 7a,  
 667 left. It shows the existence of five fibers; each fiber is also an orbit. The minimal partition obtained  
 668 by the fibers is the same as the minimal orbital partition. This implies that the group symmetry of  
 669 this graph is the same as the fibration symmetry of the graph.

670 The fibers are:

$$\begin{aligned}
 \mathcal{Fiber}_1 &= \{\text{PreMA}_L, \text{PreMA}_R\} \\
 \mathcal{Fiber}_2 &= \{\text{BA}_L, \text{BA}_R\} \\
 \mathcal{Fiber}_3 &= \{\text{AG}_L, \text{AG}_R\} \\
 \mathcal{Fiber}_4 &= \{\text{WA}_L, \text{WA}_R, \text{SMG}_L, \text{SMG}_R\} \\
 \mathcal{Fiber}_5 &= \{\text{SMA}\}
 \end{aligned}$$

671 Generally, the orbital partition obtained from automorphisms does not necessarily need to  
 672 coincide with the balanced coloring obtained from the fibration analysis. Fibers capture more  
 673 symmetries than orbits. Thus, the number of fibers is always equal to or smaller than the number  
 674 of orbits. Moreover, an orbit is always part of a fiber, but a fiber may not be part of an orbit. When  
 675 these two partitions are the same, the two symmetries are the same, too, implying a high symmetry  
 676 state.

677 The analysis of the input trees of this connectome is shown in Fig. 7c for the main fiber of  
 678 4 ROIs,  $\mathcal{Fiber}_4$  and a representative bilateral fiber  $\mathcal{Fiber}_2$ . This shows the isomorphism between  
 679 the input trees of ROIs within a fiber. This analysis complements the fibration analysis of balanced  
 680 coloring. The same analysis is done below for the RS and task-based inferred networks.

## 681 **15 Integer linear program for symmetry-driven inference of the structural network to sat-** 682 **isfy cluster synchronization**

683 The way the functioning of the brain is connected to its underlying structure adjusts according  
 684 to the requirements of the brain activity <sup>20,21</sup>. Thus, the same baseline highway can give rise  
 685 to different functional states, e.g., RS or language task of verbal and fluency, given by different  
 686 synchronized coloring patterns (e.g., Fig. 2a, c, e, respectively). Consistent with this idea, a given  
 687 functional network (at rest or task) is sustained by a specific configuration of the connectome,  
 688 in a way, strictly depends on the activity itself. A condition for such matching to exist is that a  
 689 modification of the connectome displayed in Fig. 1a is introduced. Given the baseline connectome,  
 690 which represents the communication highway, only a subset of routes are needed to guarantee the  
 691 existence of the synchronous clusters (fibers/orbits) of the functional network.

692 The crucial step of this scheme to infer the structural network from the functional network  
 693 is the fibration/group symmetry partitioning and the iterative decimation process for the coloring

694 matching. The partition problem is weakly NP-Hard <sup>76</sup>, but it has been shown that solving the  
695 directed/undirected in-balanced K-coloring problem solves the partition problem <sup>35</sup>. In particular,  
696 the problem of finding removals that satisfy the coloring condition can be formulated as a mixed  
697 integer program that is solvable for modestly sized instances. We follow a similar approach in  
698 this paper and formulate the problem of finding the minimum perturbations to induce a minimal  
699 balanced coloring as an integer linear program, i.e., an optimization problem where the decision  
700 variables are all integer. The objective and constraint functions are linear. We then solve the integer  
701 linear programs with the solver Gurobi <sup>77</sup>.

We consider a directed graph,  $G = (V, E)$ , where  $V$  denotes the set of nodes, and  $E$  denotes the set of directed edges (an undirected edge is considered as two directed edges). Also, we denote  $n = |V|$  and  $m = |E|$  as the number of nodes and directed edges, respectively. We also define

$$E^C = \{ij : i, j \in V, ij \notin E\} \quad (12)$$

702 as the set of ordered pairs of nodes for which no directed edge exists in  $G$ , which we refer to as *non-*  
703 *edges*. These ordered pairs represent potential edges that could be added to the graph  $G$ . We let  $\mathcal{S}$   
704 denote a coloring of  $G$ , i.e.,  $\mathcal{S}$  is the collection of sets partitioning  $V$ . This coloring,  $\mathcal{S}$ , is provided  
705 by the CS from fMRI synchronization in different engagements of the brain function, Fig. 2a, c, e.  
706 We define  $\alpha, \beta$  as constant parameters that govern the objective's relative importance between edge  
707 removal and edge addition. *We wish to determine the minimum number of edges to add or remove*  
708 *so that  $\mathcal{S}$  is a balanced coloring of  $G$ , i.e.,  $\mathcal{S}$  satisfies Definition 5 for  $G$ .* Our integer programs are  
709 guaranteed to find a balanced coloring but are not guaranteed to find a minimal balanced coloring.  
710 However, in our experiments, a minimal balanced coloring was found in all cases we tested.

711 The model's three families of binary decision variables are defined as follows.

712 For  $ij \in E$ ,

$$r_{ij} = 1 \text{ if edge } ij \text{ is removed, } 0 \text{ otherwise.} \quad (13)$$

For  $ij \in E^C$ ,

$$a_{ij} = 1 \text{ if non-edge } ij \text{ is added, } 0 \text{ otherwise.} \quad (14)$$

For  $P, Q, R \in \mathcal{S}$  with  $P \neq Q$  and for  $i \in P, j \in Q$

$$s_{ijR} = 1 \text{ if } i \text{ and } j \text{ are imbalanced on } R \quad (15)$$

713 and 0 otherwise. The role of the linear constraints below are to set up a set of linear equalities and  
714 inequalities that, if satisfied by these decision variables, cause the resulting perturbed graph to be  
715 a minimal balanced coloring.

716

The objective function is to minimize the weighted sum of edges removed and edges added. The function is then defined as:

$$f_{\alpha, \beta}(r, a) = \alpha \sum_{ij \in E} r_{ij} + \beta \sum_{ij \in E^C} a_{ij}. \quad (16)$$

The main constraint assures that  $\mathcal{S}$  is a balanced coloring of the perturbed graph  $G$ .

$$\begin{aligned} \sum_{ip \in E: i \in S} (1 - r_{ip}) + \sum_{ip \in E^C: i \in S} a_{ip} = \\ \sum_{iq \in E: i \in S} (1 - r_{iq}) + \sum_{iq \in E^C: i \in S} a_{iq}; p, q \in T; S, T \in \mathcal{S}. \end{aligned} \quad (17)$$

717 Constraints (17) exist for every pair of nodes  $p, q$  that are the same color and for every color  
 718 set. Note that for a given edge  $ij \in E$ , the quantity  $1 - r_{ij}$  is 1 if the edge is not removed and 0 if  
 719 it is removed. Also, for  $ij \in E^C$ , the quantity  $a_{ij}$  is 1 if  $ij$  is a newly created edge and 0 otherwise.  
 720 Thus, the left-hand side of (17) represents the edges that enter into a given node  $p$  from the color  
 721 set  $S$ , and the right-hand side represents the edges entering node  $q$  from the color set  $S$ . Using the  
 722 same sums, (18) ensure that the in-degree is at least one for every node:

$$\sum_{ip \in E} (1 - r_{ip}) + \sum_{ip} a_{ip} \geq 1, \quad p \in V. \quad (18)$$

723 The following constraints are valid for minimal balanced colorings, i.e., they are necessary  
 724 but not sufficient.

$$\begin{aligned} \sum_{ip \in E: i \in R} (1 - r_{ip}) + \sum_{ip: i \in R} a_{ip} - \\ \left( \sum_{iq \in E: i \in R} (1 - r_{iq}) + \sum_{iq: i \in R} a_{iq} \right) \geq s_{pqR} - ns_{qpR}; \\ p \in S; q \in T; R, S \neq T \in \mathcal{S}, \end{aligned} \quad (19)$$

$$\begin{aligned} \sum_{iq \in E: i \in R} (1 - r_{iq}) + \sum_{iq: i \in R} a_{iq} - \\ \left( \sum_{ip \in E: i \in R} (1 - r_{ip}) + \sum_{ip: i \in R} a_{ip} \right) \geq s_{qpR} - ns_{pqR}; \\ p \in S; q \in T; R, S \neq T \in \mathcal{S}, \end{aligned} \quad (20)$$

$$s_{pqR} + s_{qpR} \leq 1; \quad (21)$$

$$p \in S; q \in T; R, S \neq T \in \mathcal{S}, \quad (21)$$

$$\sum_{R \in \mathcal{S}} (s_{pqR} + s_{qpR}) \geq 1; \quad (22)$$

$$p \in S; q \in T; S, T \in \mathcal{S} \quad (23)$$

725 The inequalities (21) keep at most one of the two binary variables  $s_{pqR}$  to be equal to one for  
726 every color  $R$ . If both are zero, then the inequalities (19) and (20) would force  $p$  and  $q$  to be  
727 balanced for the color  $R$ . If one is zero, the total in-adjacent nodes of color  $R$  would be at least  
728 one different for  $p$  and  $q$ . In particular, for color  $R$ , if  $s_{pqR} = 1$  and  $s_{qpR} = 0$ , then the number of  
729 in-adjacent nodes to  $p$  is at least one greater than that to color  $q$ . The converse is also true. The  
730 inequalities (23) force that one of  $s_{pqR}$  or  $s_{qpR}$  is equal to one for at least one color  $R$ . This is a  
731 necessary but not sufficient condition for the coloring to be *minimal*. For example, if two color  
732 partitions have no edges between them, the same number of edges to all other colors, and the same  
733 positive number of internal edges, then (23) is satisfied as their different colors will register as an  
734 imbalance. However, the union of these two color partitions is balanced and has one less color,  
735 i.e., the coloring is no longer minimal. That being said, our experiments yielded strong evidence  
736 that the necessary condition sufficiently enforces the minimal balanced condition in practice, as  
737 we found a minimal balanced coloring for all of our test cases.

The complete model is then:

$$\begin{aligned}
& \min f_{\alpha,\beta}(r, a) \\
& \text{subject to} \quad (17), (18), (20), (20), (21), (23), \\
& \quad r_{ij}, a_{k\ell}, s_{pqR} \in \{0, 1\}, ij \in E, \\
& \quad k\ell \in E^C, p \in P, q \in Q, P \neq Q, R \in \mathcal{S}.
\end{aligned} \tag{24}$$

738 where Eq. (23) within equation above is a reference to select only one of its sub-equations.

739 The uniqueness of the solution is tested by developing an independent solver based on the  
740 quasi-fibration framework developed in <sup>36</sup>. In all cases considered, we find the same solution using  
741 the quasi-fibration formalism and MILP.

742 Due to its large complexity, the brain can never have exact symmetries, even within a single  
743 connectome. Structural brains are all different, but a certain level of ideal symmetry must be  
744 common to all of them to guarantee the performance of an average synchronization pattern, despite  
745 not all structural brains being identical. We apply the inference algorithms to those group-average  
746 synchronization networks and connectomes at the mesoscopic level, as shown in Figs. 2 and 4  
747 which should be interpreted as idealized networks.

## 748 16 Symmetry breaking in physics and the brain

749 Most symmetry laws in physics are broken in one way or another. One such mechanism is sponta-  
750 neous symmetry breaking, where the laws of physics remain symmetric, but the system's ground  
751 state exhibits a lower symmetry than the full system, as in a paramagnetic-to-ferromagnetic phase  
752 transition <sup>39</sup>. For temperatures below the critical value  $T_C$ , the magnetic moments of the atoms of  
753 ferromagnetic material are partially aligned within magnetic domains, producing a net magnetic  
754 moment even though the atoms interact through a spin-spin interaction, which is invariant under  
755 rotation. Thus, the rotational invariant symmetry of the system is broken into this ground state

756 with a non-zero magnetic moment. As the temperature increases, this alignment is destroyed by  
757 thermal fluctuations and the net magnetization progressively reduces until vanishing at  $T_C$ . The  
758 orientation of the magnetization is random. Each possible direction is equally likely to occur, but  
759 only one is chosen at random, resulting in a zero net magnetic moment. So, the rotational symme-  
760 try of the ferromagnet is manifest for  $T > T_C$  with zero magnetic moment, but is broken by the  
761 arbitrary selection of a particular (less-symmetrical) ground state with non-zero magnetic moment  
762 for  $T < T_C$ .

763 Another type is explicit symmetry breaking, where the dynamics are only approximately  
764 symmetric, yet the deviation caused by the breaking forces is minimal. Hence, one can consider  
765 the symmetry violation as a small correction in the system. An example is the spectral line splitting  
766 in the Zeeman effect due to a magnetic interaction perturbation in the Hamiltonian of the atoms  
767 involved.

768 In the present work, we implemented a symmetry-driven algorithm based on a mixed integer  
769 linear program to infer the structural network associated with each balanced coloring of the func-  
770 tional network obtained experimentally in different tasks. By applying this novel framework to  
771 healthy subjects performing standard language tasks, we obtained a functional language anatomy  
772 which is consistent with the common understanding of speech processing.

773 The symmetry-breaking we find in the brain is manifested in the following:

- 774 1. The evidence of an underlying highly symmetrical connectome between the language areas  
775 (group symmetry = fibration symmetry) with a novel central fiber made of 4 ROIs.
- 776 2. The evidence of a symmetrical language network representation during resting state as a  
777 consequence of the overall synchronization dynamics with a novel pentagonal fiber at the  
778 core of the network made of SMA, PreMA and WA. This network presents only fibration  
779 symmetries but no group symmetries thus, the resting state engagement breaks the global  
780 group symmetries of the baseline connectome. That is, even though the ROIs are synchro-  
781 nized in pairs with left-right symmetry, the underlying structural network does not have the  
782 global left-right symmetry. In fact, it has no automorphisms at all. This is remarkable. The  
783 only surviving symmetry is the local fibration.
- 784 3. The characterization of the transition between resting state and language tasks as further  
785 broken symmetry, but this time of the fibration symmetry (the group symmetry remains  
786 broken). The evidence of a breaking of symmetry resulting in two novel central fibers (BA  
787 L-SMA) and (WA L-WA R-BR R).
- 788 4. The evidence of slightly different engagement of the comprehension center formed by fronto-  
789 temporal-parietal language areas in the phonemic fluency and verb generation tasks sup-  
790 ported by the same pattern of communication routes, i.e., the same structural connectivity.  
791 Thus, while the communication routes are the same for the two tasks, frontal and parietal

792 regions are characterized by different levels of bilateral synchronization (different rearrange-  
793 ment to communication) according to the task executed: frontal area is more synchronized  
794 during verb generation, and parietal areas are more synchronized during noun generation.

- 795 5. Possible applications will include the analysis of broken symmetries in neurological dis-  
796 orders and correlation with patients' clinical performance. Some neurological conditions  
797 compromise the synchronization in the brain (tumors, stroke, any focal lesion), affecting its  
798 coherent activity. By applying our method to these patients, we could shed light on bio-  
799 markers that could predict symptoms and patients' prognosis.

## 800 17 Analysis of symmetries of the RS structural network

801 We perform a full symmetry analysis (group and fibration symmetry) of the inferred resting state  
802 structural network in Fig. 8.

First, McKay's Nauty algorithm<sup>52</sup> is used to calculate the automorphisms of the network. Out of the  $11! = 39,916,800$  possible permutations of its 11 ROIs only the identity [ $\pi_0 = \text{Id}$ ] is an automorphism (Fig. 8b, left). Any other permutation is not a symmetry. For instance, if we implement the permutation

$$\pi_2 = (\text{WA}_L \text{SMG}_L) (\text{WA}_R \text{SMG}_R), \quad (25)$$

803 we obtain a different graph (Fig. 8b, right).

804 Accordingly, the resting state structural network has only trivial group symmetry. Colloqui-  
805 ally, we say that this network has no group symmetry. Since the only automorphism is the trivial  
806 identity, each node has its orbit. Thus, there are eleven orbits: one for each node, Fig. 8a, right. If  
807 compared to the baseline connectome that shows five orbits, Fig. 7a right, this represents a group  
808 symmetry breaking.

809 The fibration symmetry analysis is done by finding the balanced coloring (fibers) using the  
810 refinement algorithm of Kamei and Cock<sup>51</sup> and Morone *et al.*<sup>18</sup>. Figure 8a left shows the resulting  
811 minimal balanced coloring. When compared to the baseline connectome Fig. 7a left, an increase  
812 of fibration symmetry is obtained since now we observed a smaller number of fibers. Recall that  
813 the most symmetric graph is that with a single color, and the least symmetric graph is the one with  
814  $N$  colors for a graph with  $N$  nodes. While in the baseline, we have five fibers, in the resting state  
815 the number of fibers is four.

816 When compared to the orbital partition of the same graph, Fig. 8a, right, we find that this  
817 graph has fibration symmetry but no group symmetry. The global symmetry has been fully bro-  
818 ken by engaging the brain in RS, but the local symmetry remains, and it is enhanced in RS in  
819 comparison to the original symmetry of the connectome.

820 The fibers are:

$$\begin{aligned}
\mathcal{Fiber}_1 &= \{\text{SMA}, \text{PreMA}_L, \text{PreMA}_R, \text{WA}_L, \text{WA}_R\} \\
\mathcal{Fiber}_2 &= \{\text{BA}_L, \text{BA}_R\} \\
\mathcal{Fiber}_3 &= \{\text{AG}_L, \text{AG}_R\} \\
\mathcal{Fiber}_4 &= \{\text{SMG}_L, \text{SMG}_R\}
\end{aligned}$$

821 The analysis of the input trees is shown in Fig. 8c for the main fiber of 5 ROIs,  $\mathcal{Fiber}_1$  and  
822 a representative bilateral fiber  $\mathcal{Fiber}_3$ . This complements the fibration analysis of this graph.

## 823 18 Analysis of symmetries of the task structural network

824 We perform a full symmetry analysis (including group and fibration symmetry) of the inferred task  
825 structural network in Fig. 9.

Similar to the RS network, McKay’s Nauty algorithm<sup>52</sup> shows that this graph has no auto-  
morphisms except for the trivial identity. From the 11! allowed permutations, only the identity  
 $[\pi_0 = \text{Id}]$  is a symmetry (Fig. 9b, left). For instance, if we implement the permutation

$$\pi_1 = (\text{PreMA}_L \text{PreMA}_R) (\text{BA}_L \text{BA}_R) (\text{AG}_L \text{AG}_R) (\text{WA}_L \text{WA}_R) (\text{SMG}_L \text{SMG}_R) \quad (26)$$

826 we obtain a different graph (Fig. 9b, right), exactly as we found for in RS (Fig. 8b).

827 Since there are no (non-trivial) automorphisms, we obtain eleven orbits (one for each node,  
828 Fig. 9a, right) for the task network as in RS. Thus, the baseline connectome’s global symmetry  
829 remains broken in the language task.

830 The fibration symmetry analysis for this connectome gives rise to a the balanced coloring  
831 partition seen in Fig. 9a, left. We found five fibers:

$$\begin{aligned}
\mathcal{Fiber}_1 &= \{\text{SMA}, \text{BA}_L\} \\
\mathcal{Fiber}_2 &= \{\text{PreMA}_L, \text{PreMA}_R\} \\
\mathcal{Fiber}_3 &= \{\text{AG}_L, \text{AG}_R\} \\
\mathcal{Fiber}_4 &= \{\text{BA}_R, \text{WA}_L, \text{WA}_R\} \\
\mathcal{Fiber}_5 &= \{\text{SMG}_L, \text{SMG}_R\}
\end{aligned}$$

832 If compared to the resting state connectome Fig. 8a, a decrease of fibration symmetry is ob-  
833 tained. In RS, we have four fibers, and in the task, we have five. This represents a fibration  
834 symmetry breaking (more fibers means less fibration symmetry). This local symmetry breaking

835 is the product of the breaking of left-right local symmetry in the Broca area due to language lat-  
836 eralization. Recall that the left-right global symmetry has been fully broken in the RS state and  
837 remains broken here. This local breaking of symmetry is done by the synchronization of Broca left  
838 with SMA, and the independent synchronization of Broca right to Wernicke left and right. These  
839 two areas remain locally left-right symmetric. This produces the main two fibers controlling the  
840 language network  $Fiber_1$  and  $Fiber_4$ . The analysis of the input trees of these fibers is shown in  
841 Fig. 9c.

842 **Acknowledgments** Funding for this project was provided by NIBIB and NIMH through the NIH BRAIN  
843 Initiative Grant R01 EB028157 to M.Z. and H.A.M. P.B. was partially funded by the project SERICS  
844 (PE00000014) under the NRRP MUR program funded by the EU - NGEU. T.G. thankfully acknowledges  
845 financial support by the European Union - NextGenerationEU - National Recovery and Resilience Plan  
846 (Piano Nazionale di Ripresa e Resilienza, PNRR), project ‘SoBigData.it - Strengthening the Italian RI for  
847 Social Mining and Big Data Analytics’ - Grant IR0000013 (n. 3264, 28/12/2021). We thank G. Del Ferraro  
848 and Luis Alvarez for discussions.

849 **Code availability** All code and data to reproduce the results of this paper are available at [https://](https://github.com/MakseLab)  
850 [github.com/MakseLab](https://github.com/MakseLab) and <https://osf.io/4ern8/>

851 **Competing Interests** The authors declare that they have no competing financial interests.

852 **Correspondence** Correspondence and requests for materials should be addressed to H.A.M.  
853 (email: [hmakse@ccny.cuny.edu](mailto:hmakse@ccny.cuny.edu)).

854 **References**

- 855 1. Wilczek, F. *A Beautiful Question: Finding Nature's Deep Design* (Penguin, 2016).
- 856 2. Weinberg, S. *The Quantum Theory of Fields*, vol. 2 (Cambridge U.P., 1995).
- 857 3. Georgi, H. *Lie Algebras in Particle Physics: From Isospin to Unified Theories* (Taylor &  
858 Francis, 2000).
- 859 4. Chaikin, P. M. & Lubensky, T. C. *Principles of Condensed Matter Physics* (Cambridge U.P.,  
860 Cambridge, 1995).
- 861 5. Monod, J. Symmetry and function of biological systems at the macromolecular level. *Proc.*  
862 *11th Nobel Symposium, Södergarn, Lidingö, Sweden, Aug. 1968. A. Engström and B. Strand-*  
863 *berg, Eds. Interscience (Wiley), New York, and Almqvist and Wiksell, Stockholm, 1969. pp. 436*  
864 *(1970).*
- 865 6. Grothendieck, A. Technique de descente et théorèmes d'existence en géométrie algébrique,  
866 I. Généralités. Descente par morphismes fidèlement plats. *Seminaire Bourbaki* **190** (1959–  
867 1960).
- 868 7. Anderson, P. W. More is different: Broken symmetry and the nature of the hierarchical struc-  
869 ture of science. *Science* **177**, 393–396 (1972).
- 870 8. Barzel, B. & Barabási, A.-L. Universality in network dynamics. *Nat. Phys.* **9**, 673–681 (2013).
- 871 9. Arenas, A., Díaz-Guilera, A., Kurths, J., Moreno, Y. & Zhou, C. Synchronization in complex  
872 networks. *Phys. Rep.* **469**, 93–153 (2008).
- 873 10. Pecora, L. M., Sorrentino, F., Hagerstrom, A. M., Murphy, T. E. & Roy, R. Cluster synchro-  
874 nization and isolated desynchronization in complex networks with symmetries. *Nat. Commun.*  
875 **5**, 4079 (2014).
- 876 11. Sorrentino, F., Pecora, L. M., Hagerstrom, A. M., Murphy, T. E. & Roy, R. Complete charac-  
877 terization of the stability of cluster synchronization in complex dynamical networks. *Sci. Adv.*  
878 **2**, e1501737 (2016).
- 879 12. Golubitsky, M. & Stewart, I. Nonlinear dynamics of networks: the groupoid formalism. *BAMS*  
880 **43**, 305–364 (2006).
- 881 13. Stewart, I., Golubitsky, M. & Pivato, M. Symmetry groupoids and patterns of synchrony in  
882 coupled cell networks. *SIAM J. Appl. Dyn. Syst.* **2**, 609–646 (2003).
- 883 14. Boldi, P. & Vigna, S. Fibrations of graphs. *Discrete Math.* **243**, 21–66 (2002).
- 884 15. DeVille, L. & Lerman, E. Modular dynamical systems on networks. *J. Eur. Math. Soc.* **17**,  
885 2977–3013 (2015).

- 886 16. Nijholt, E., Rink, B. & Sanders, J. Graph fibrations and symmetries of network dynamics.  
887 *Diff. Equ.* **261**, 4861–4896 (2016).
- 888 17. Morone, F. & Makse, H. A. Symmetry group factorization reveals the structure-function  
889 relation in the neural connectome of caenorhabditis elegans. *Nat. Commun.* **10**, 4961 (2019).
- 890 18. Morone, F., Leifer, I. & Makse, H. A. Fibration symmetries uncover the building blocks of  
891 biological networks. *Proc. Nat. Acad. Sci. USA* **117**, 8306–8314 (2020).
- 892 19. Leifer, I. *et al.* Circuits with broken fibration symmetries perform core logic computations in  
893 biological networks. *PLoS Comput. Biol.* **16**, e1007776 (2020).
- 894 20. Park, H.-J. & Friston, K. Structural and functional brain networks: from connections to cog-  
895 gnition. *Science* **342**, 1238411 (2013).
- 896 21. Friston, K. J. Functional and effective connectivity: a review. *Brain Connect.* **1**, 13–36 (2011).
- 897 22. Bullmore, E. & Sporns, O. Complex brain networks: graph theoretical analysis of structural  
898 and functional systems. *Nat. Rev. Neurosci.* **10**, 186–198 (2009).
- 899 23. Honey, C. J. *et al.* Predicting human resting-state functional connectivity from structural  
900 connectivity. *Proc. Nat. Acad. Sci. USA* **106**, 2035–2040 (2009).
- 901 24. Friederici, A. D. The brain basis of language processing: from structure to function. *Physiol.*  
902 *Rev.* (2011).
- 903 25. Koch, M. A., Norris, D. G. & Hund-Georgiadis, M. An investigation of functional and anatom-  
904 ical connectivity using magnetic resonance imaging. *Neuroimage* **16**, 241–250 (2002).
- 905 26. Greicius, M. D., Supekar, K., Menon, V. & Dougherty, R. F. Resting-state functional con-  
906 nectivity reflects structural connectivity in the default mode networ. *Cereb. Cortex* **19**, 72–78  
907 (2009).
- 908 27. van den Heuvel, M. P., Mandl, R. C. W., Kahn, R. S. & Hulshoff Pol, H. E. Functionally  
909 linked resting-state networks reflect the underlying structural connectivity architecture of the  
910 human brain. *Hum. Brain Mapp.* **30**, 3127–3141 (2009).
- 911 28. Deco, G. *et al.* Resting-state functional connectivity emerges from structurally and dynami-  
912 cally shaped slow linear fluctuations. *J. Neurosci.* **33**, 11239–11252 (2013).
- 913 29. Wein, S. *et al.* Brain connect studies on structure-function relationships: A short survey with  
914 an emphasis on machine learning. *Comput. Intell. Neurosci.* **2021** (2021).
- 915 30. Pang, J. C. *et al.* Geometric constraints on human brain function. *Nature* **618**, 566–574 (2023).
- 916 31. Weyl, H. *Symmetry*. Princeton Science Library (Princeton U.P., 1952).

- 917 32. Bronstein, M. M., Bruna, J., Cohen, T. & Velicković, P. Geometric deep learning: Grids,  
918 groups, graphs, geodesics, and gauges. *arXiv preprint arXiv:2104.13478* (2021).
- 919 33. Leifer, I., Sánchez-Pérez, M., Ishida, C. & Makse, H. A. Predicting synchronized gene co-  
920 expression patterns from fibration symmetries in gene regulatory networks in bacteria. *BMC*  
921 *Bioinf.* **22**, 1–34 (2021).
- 922 34. Avila, B., Serafino, M., Augusto, P., Zimmer, M. & Makse, H. A. Fibration symmetries and  
923 cluster synchronization in the *c. elegans* connectome. *PLoS ONE* **19**(4), e0297669 (2024).
- 924 35. Leifer, I., Phillips, D., Sorrentino, F. & Makse, H. A. Symmetry-driven network reconstruction  
925 through pseudobalanced coloring optimization. *J. Stat. Mech.: Theor. Exp.* **2022**, 073403  
926 (2022).
- 927 36. Boldi, P., Leifer, I. & Makse, H. A. Quasifibrations of graphs to find symmetries and recon-  
928 struct biological networks. *J. Stat. Mech.: Theor. Exp.* **2022**, 113401 (2022).
- 929 37. Xu, K., Hu, W., Leskovec, J. & Jegelka, S. How powerful are graph neural networks? *arXiv*  
930 *preprint arXiv:1810.00826* (2018).
- 931 38. Velarde, O., Parra, L., Boldi, P. & Makse, H. A. The role of fibration symmetries in geometric  
932 deep learning. *ArXiv* (2024).
- 933 39. Yeomans, J. M. *Statistical Mechanics of Phase Transitions* (Clarendon Press, 1992).
- 934 40. Li, Q. *et al.* Core language brain network for fmri language task used in clinical applications.  
935 *Network Neurosci.* **4**, 134–154 (2020).
- 936 41. Azeez, A. K. & Biswal, B. B. A review of resting-state analysis methods. *Neuroimaging Clin.*  
937 **27**, 581–592 (2017).
- 938 42. Hickok, G. & Poeppel, D. The cortical organization of speech processing. *Nat. Rev. Neurosci.*  
939 **8**, 393–402 (2007).
- 940 43. Hickok, G. The dual stream model of speech and language processing. *Handbook of Clinical*  
941 *Neurology* **185**, 57–69 (2022).
- 942 44. Bruña, R., Maestú, F. & Pereda, E. Phase locking value revisited: teaching new tricks to an  
943 old dog. *J. Neural. Eng.* **15**, 056011 (2018).
- 944 45. Gallos, L. K., Makse, H. A. & Sigman, M. A small world of weak ties provides optimal global  
945 integration of self-similar modules in functional brain networks. *Proc. Nat. Acad. Sci. USA*  
946 **109**, 2825–2830 (2012).
- 947 46. Mastrandrea, R. *et al.* Information load dynamically modulates functional brain connect dur-  
948 ing narrative listening. *Sci. Rep.* **13**, 8110 (2023).

- 949 47. Teghipco, A., Hussain, A. & Tivarus, M. E. Disrupted functional connectivity affects resting  
950 state based language lateralization. *NeuroImage Clin.* **12**, 910–927 (2016).
- 951 48. Seitzman, B. A., Snyder, A. Z., Leuthardt, E. C. & Shimony, J. S. The state of resting state  
952 networks. *Top. Magn. Reson. Imaging* **28**, 189 (2019).
- 953 49. Dixon, J. D. & Mortimer, B. *Permutation Groups, Graduate Texts in Mathematics*, vol. 163  
954 (Springer New York, 1996).
- 955 50. Aldis, J. W. A polynomial time algorithm to determine maximal balanced equivalence rela-  
956 tions. *Int. J. Bifurcat. Chaos* **18**, 407–427 (2008).
- 957 51. Kamei, H. & Cock, P. J. Computation of balanced equivalence relations and their lattice for a  
958 coupled cell network. *SIAM J. Appl. Dyn. Syst.* **12**, 352–382 (2013).
- 959 52. McKay, B. D. & Piperno, A. Practical graph isomorphism, ii. *ArXiv* (2013). URL <https://arxiv.org/pdf/1301.1493.pdf>.  
960
- 961 53. Dick, A. S., Bernal, B. & Tremblay, P. The language connectome: new pathways, new con-  
962 cepts. *Neuroscientist* **20**, 453–467 (2014).
- 963 54. Chang, E. F., Raygor, K. P. & Berger, M. S. Contemporary model of language organization:  
964 an overview for neurosurgeons. *J. Neurosurg.* **122**, 250–261 (2015).
- 965 55. Catani, M. *et al.* A novel frontal pathway underlies verbal fluency in primary progressive  
966 aphasia. *Brain* **136**, 2619–2628 (2013).
- 967 56. Jenabi, M., Peck, K. K., Young, R. J., Brennan, N. & Holodny, A. I. Probabilistic fiber tracking  
968 of the language and motor white matter pathways of the supplementary motor area (sma) in  
969 patients with brain tumors. *J. Neuroradiol.* **41**, 342–349 (2014).
- 970 57. Lyo, J. K., Arevalo-Perez, J., Petrovich Brennan, N., Peck, K. K. & Holodny, A. I. Pre-  
971 operative fmri localization of the supplementary motor area and its relationship with postop-  
972 erative speech deficits. *J. Neuroradiol.* **28**, 281–288 (2015).
- 973 58. Rech, F. *et al.* A probabilistic map of negative motor areas of the upper limb and face: a brain  
974 stimulation study. *Brain* **142**, 952–965 (2019).
- 975 59. Bertsimas, D. & Tsitsiklis, J. N. *Introduction to Linear Optimization*, vol. 6 (Athena Scient.  
976 Belmont, MA, 1997).
- 977 60. Friederici, A. D. & Gierhan, S. M. The language network. *Curr. Opin. Neurobio.* **23**, 250–254  
978 (2013).
- 979 61. Roger, E. *et al.* Unraveling the functional attributes of the language connectome: crucial  
980 subnetworks, flexibility and variability. *NeuroImage* **263**, 119672 (2022).

- 981 62. Toga, A. W. & Thompson, P. M. Mapping brain asymmetry. *Nat. Rev. Neurosci.* **4**, 37–48  
982 (2003).
- 983 63. Geschwind, N. Wernicke’s contribution to the study of aphasia. *Cortex* **3**, 449–463 (1967).
- 984 64. Hertrich, I., Dietrich, S. & Ackermann, H. The role of the supplementary motor area for  
985 speech and language processing. *Neurosci. & Biobehav. Rev.* **68**, 602–610 (2016).
- 986 65. Chang, W. *et al.* Representing linguistic communicative functions in the premotor cortex.  
987 *Cereb. Cortex* **33**, 5671–5689 (2023).
- 988 66. Lachaux, J.-P., Rodriguez, E., Martinerie, J. & Varela, F. J. Measuring phase synchrony in  
989 brain signals. *Hum. Brain Mapp.* **8**, 194–208 (1999).
- 990 67. Winkler, A. M., Ridgway, G. R., Douaud, G., Nichols, T. E. & Smith, S. M. Faster permutation  
991 inference in brain imaging. *Neuroimage* **141**, 502–516 (2016).
- 992 68. Winkler, A. M., Ridgway, G. R., Webster, M. A., Smith, S. M. & Nichols, T. E. Permutation  
993 inference for the general linear model. *Neuroimage* **92**, 381–397 (2014).
- 994 69. Hickok, G., Houde, J. & Rong, F. Sensorimotor integration in speech processing: computa-  
995 tional basis and neural organization. *Neuron* **69**, 407–422 (2011).
- 996 70. Li, Y. *et al.* Lexical-semantic search under different covert verbal fluency tasks: an fmri study.  
997 *Front. Behav. Neurosci.* **11**, 131 (2017).
- 998 71. Corrivetti, F. *et al.* Dissociating motor–speech from lexico-semantic systems in the left frontal  
999 lobe: insight from a series of 17 awake intraoperative mappings in glioma patients. *Brain*  
1000 *Struc. Funct.* **224**, 1151–1165 (2019).
- 1001 72. Unadkat, P. *et al.* Functional mri task comparison for language mapping in neurosurgical  
1002 patients. *J. Neuroimg.* **29**, 348–356 (2019).
- 1003 73. Aschbacher, M. *Finite Group Theory*, vol. 10 (Cambridge U.P., 2000).
- 1004 74. van Geemen, K., Herbet, G., Moritz-Gasser, S. & Duffau, H. Limited plastic potential of  
1005 the left ventral premotor cortex in speech articulation: evidence from intraoperative awake  
1006 mapping in glioma patients. *Hum. Brain Mapp.* **35**, 1587–1596 (2014).
- 1007 75. Naidich, T. P., Castillo, M., Cha, S. & Smirniotopoulos, J. G. *Imaging of the brain: expert*  
1008 *radiology series* (Elsevier Health Sci., 2012).
- 1009 76. Garey, M. R. & Johnson, D. S. “strong”np-completeness results: Motivation, examples, and  
1010 implications. *JACM* **25**, 499–508 (1978).
- 1011 77. Gurobi Optimization, LLC. Gurobi Optimizer Reference Manual (2023). URL [https:](https://www.gurobi.com)  
1012 [//www.gurobi.com](https://www.gurobi.com).

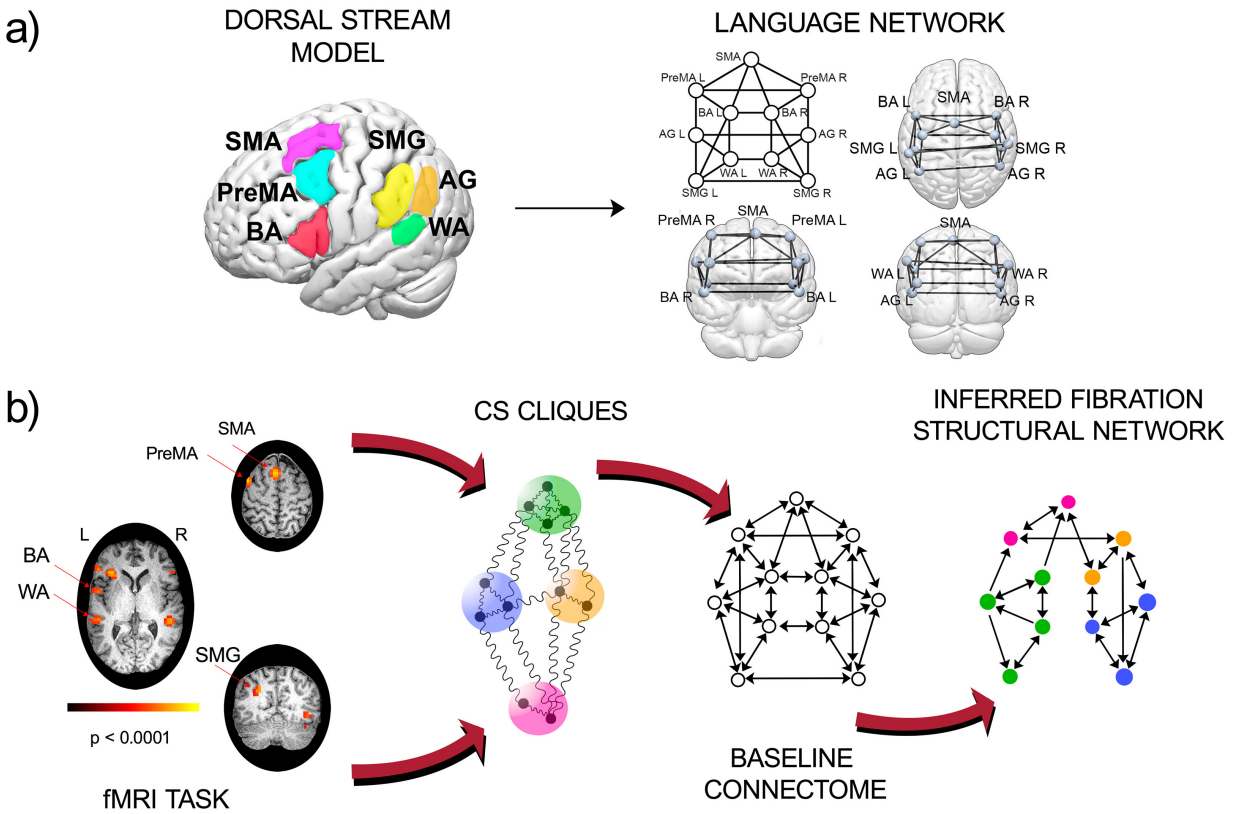


Figure 1: **Dual stream model of language and the inference scheme.** (a) Left: ROIs of the primary language network is given by the dorsal stream of the dual-stream model localized in the 3d brain. Right: dual (dorsal) stream baseline connectome showing the fiber tracks between the ROIs in (a). (b) Pipeline for inference of the structural network from CS data. Left: fMRI images for RS or a task over many subjects are taken as input to calculate the group-average CS cliques among ROIs. The CS are identified with the colors in the baseline connectome. A mixed integer programming algorithm is employed to optimally infer the structural network (right) that sustains the coloring cluster pattern obtained from the dynamics.

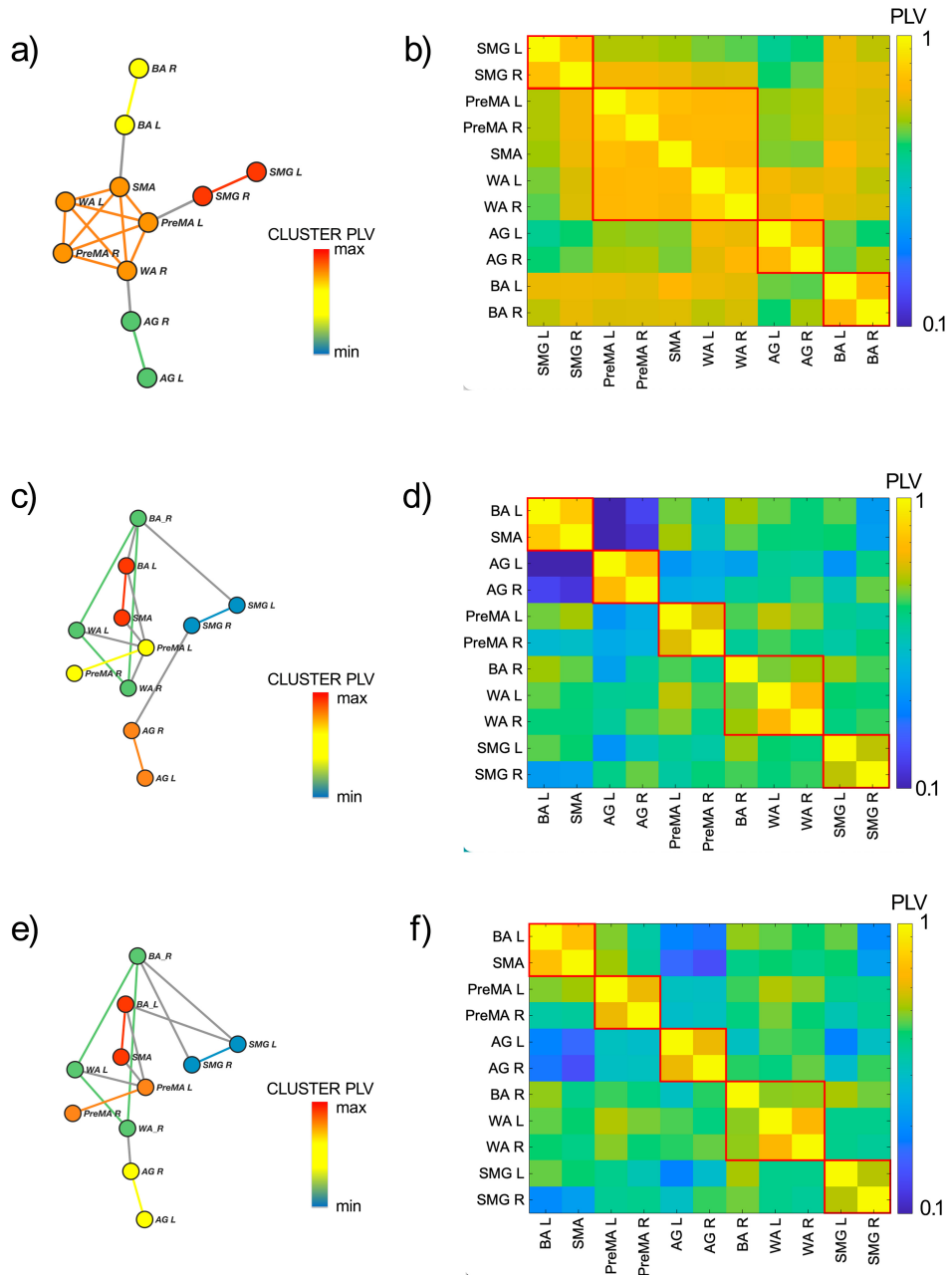
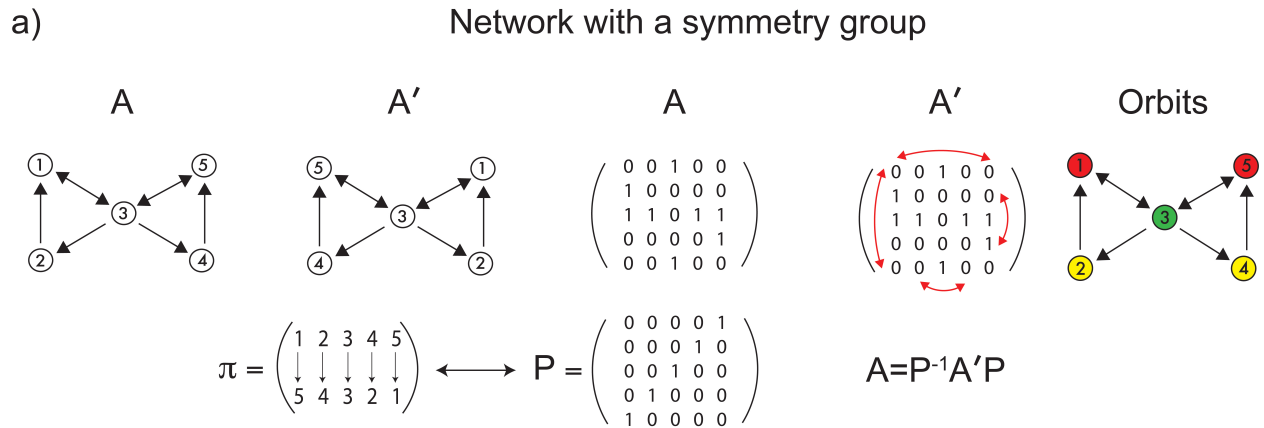


Figure 2: **Functional networks and cluster synchronization.** (a) Functional network during resting state shows the CS in different colors. (b) Phase Locking Value matrix for the eleven ROIs during resting state. (c) Functional network during phonemic fluency language. (d) Phase Locking Value matrix during phonemic fluency task. (e) Functional network during the verb generation language task. (f) Phase Locking Value matrix during verb generation task. In the three networks (a), (c) and (d) nodes and edges are colored according to the Cluster PLV color bar reported aside. Cluster PLV is calculated as the average PLV over links for each CS found in the network. Grey edges connect clusters. The red-lined boxes in (b), (d) and (e) are visual indicators for the CS and clusters are shown in decreasing order of Cluster PLV.



b) Network with no symmetry group and a fibration symmetry

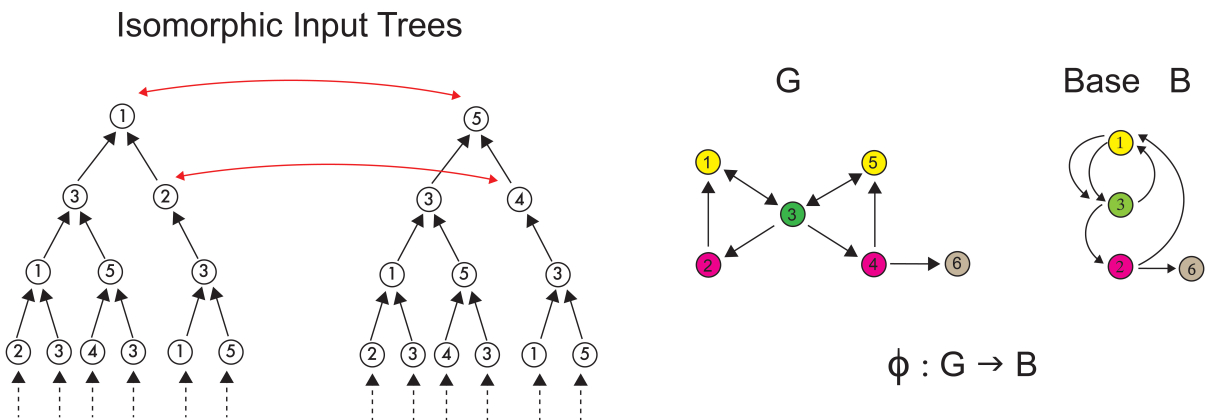
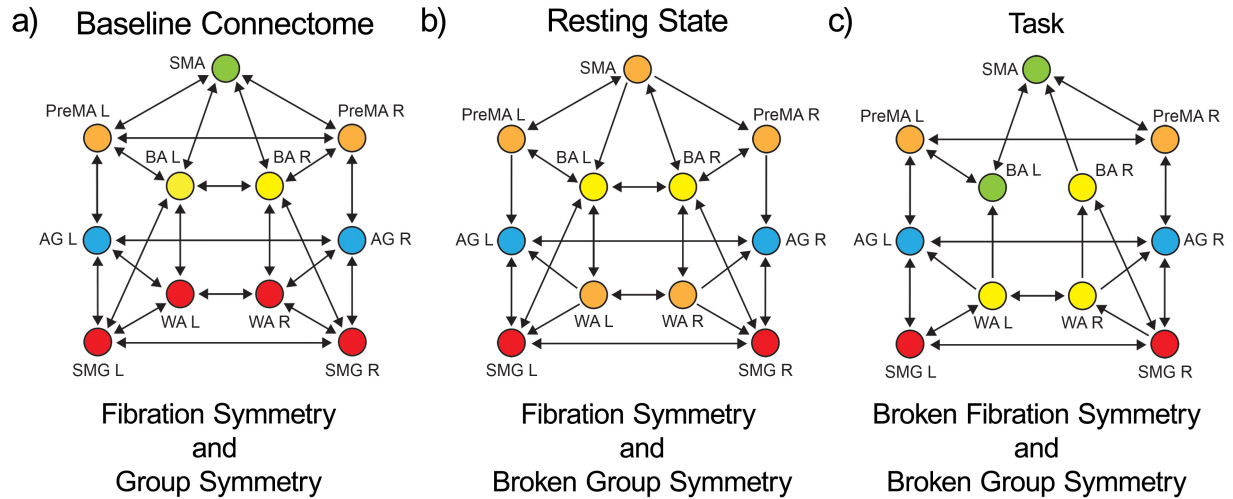


Figure 3: **Symmetry Formalism.** (a) Example of automorphism in a graph with group symmetry. Left: A permutation  $\pi$  transforms the graph  $A$  into  $A'$ . This can be written down in matrix notation through a permutation matrix  $P$ . The permutation is a symmetry when  $A = A'$ . Right: applying all symmetries to every node generates the orbital partition shown in the colored nodes. (b) Example of fibration symmetry in a graph with no group symmetry. The addition of the outgoing edge from node 4 to 6 in (b) destroys the global automorphism in (a). Yet, the symmetry fibration still remains since there are nodes (nodes 1 and 5 and nodes 2 and 4) with isomorphic input trees (left). The fiber partition is shown in graph  $G$ : (i) nodes with the same colors are in fibers, (ii) are balanced because they receive the same colors from neighbors, and (iii) are synchronized under any dynamics. The fibration  $\phi$  collapses the fibers into the base  $B$  by following the lifting property (right).



PreMA L: Premotor Left    BA L: Broca's Area Left    AG L: Angular Gyrus Left    WA L: Wernicke's Area Left    SMG L: Supramarginal Gyrus Left  
 PreMA R: Premotor Right    BA R: Broca's Area Right    AG R: Angular Gyrus Right    WA R: Wernicke's Area Right    SMG R: Supramarginal Gyrus Right  
 SMA: Supplementary Motor Area

**Figure 4: Breaking of symmetry from the baseline connectome to inferred RS network to task network.** (a) Minimal balanced coloring in the baseline connectome. This network has the highest symmetry: a global automorphism group, which is the same as the local fibration symmetry with five orbits equal to fibers (five balanced colors). (b) Inferred RS structural network using the CS from Fig. 2a. The network has only local fibration symmetry with four fibers but no global symmetry, which is broken with respect to the connectome in (a) under the RS dynamics. (c) Inferred language task network from the coloring in Fig. 2c or e (which are the same). The lateralization of function under the language task breaks the fibration symmetry of (b) showing less symmetry (more fibers than RS). The group symmetry remains broken.

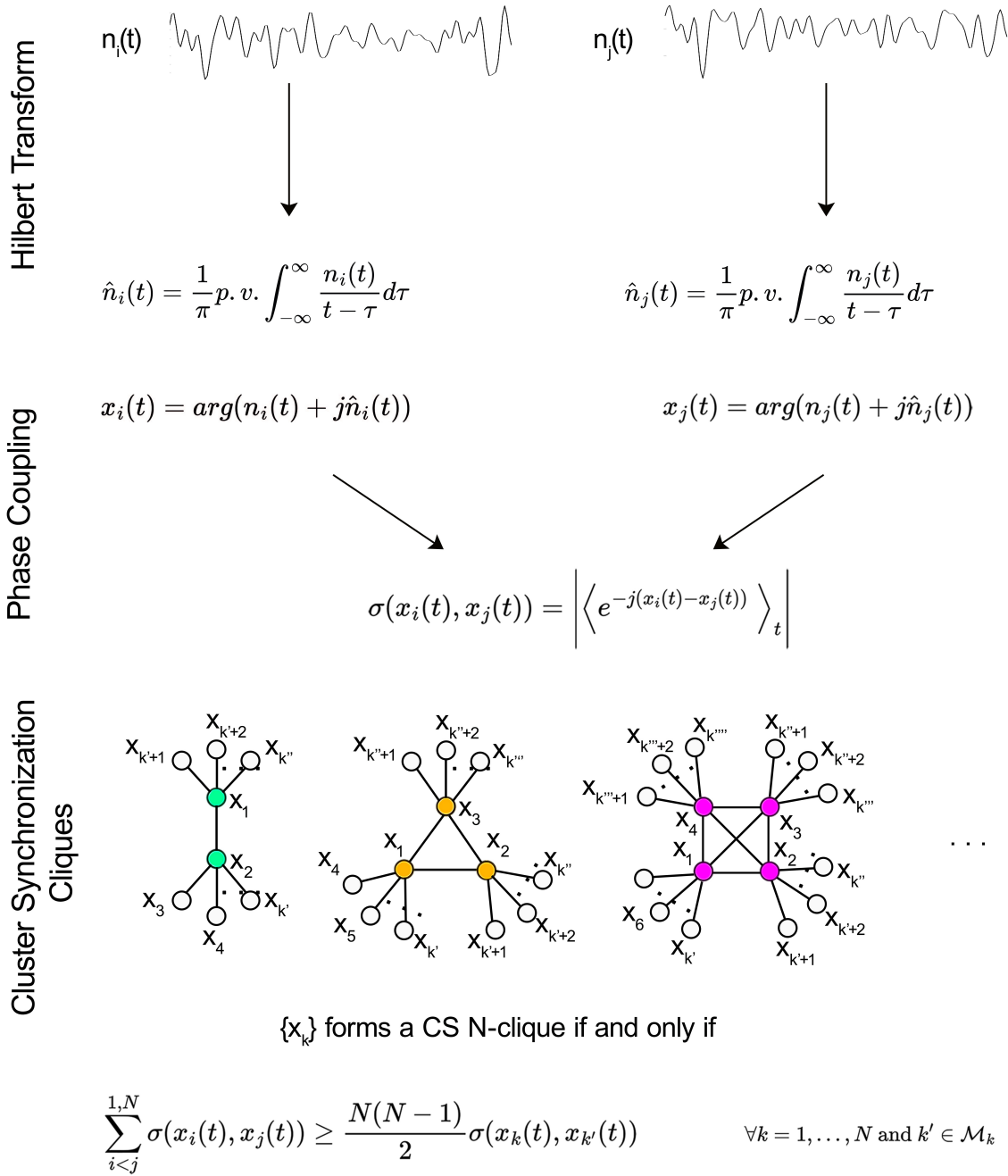


Figure 5: **Extended Data Fig. 5. Schematics of the synchronization clustering algorithm.** Pairs of time series coming from pairs of cerebral ROIs are Hilbert transformed and entered in the phase-locking value calculation. Once all the pairs of regions of interest are included in the calculation, the synchronization clustering algorithm is implemented.

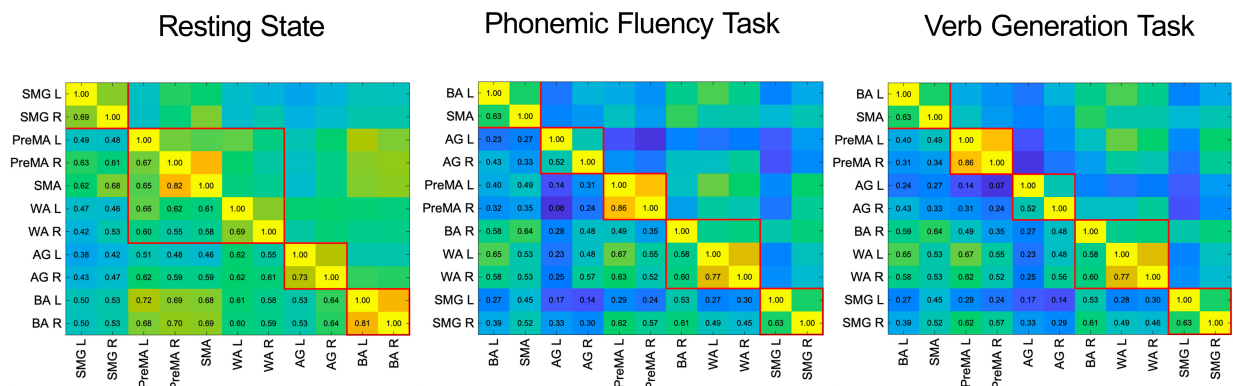


Figure 6: **Extended Data Fig. 6. Single subject phase locking value matrices.** (a) Phase locking value matrix for the resting state condition for a typical subject. (b) Phase locking value matrix for the phonemic fluency task condition. (c) Phase locking value matrix for the verb generation task condition. The red-lined boxes are visual indicators for the CS, and clusters are shown according to the order used for the average matrices shown in Fig. 2.

## Symmetry analysis of dorsal stream baseline connectome

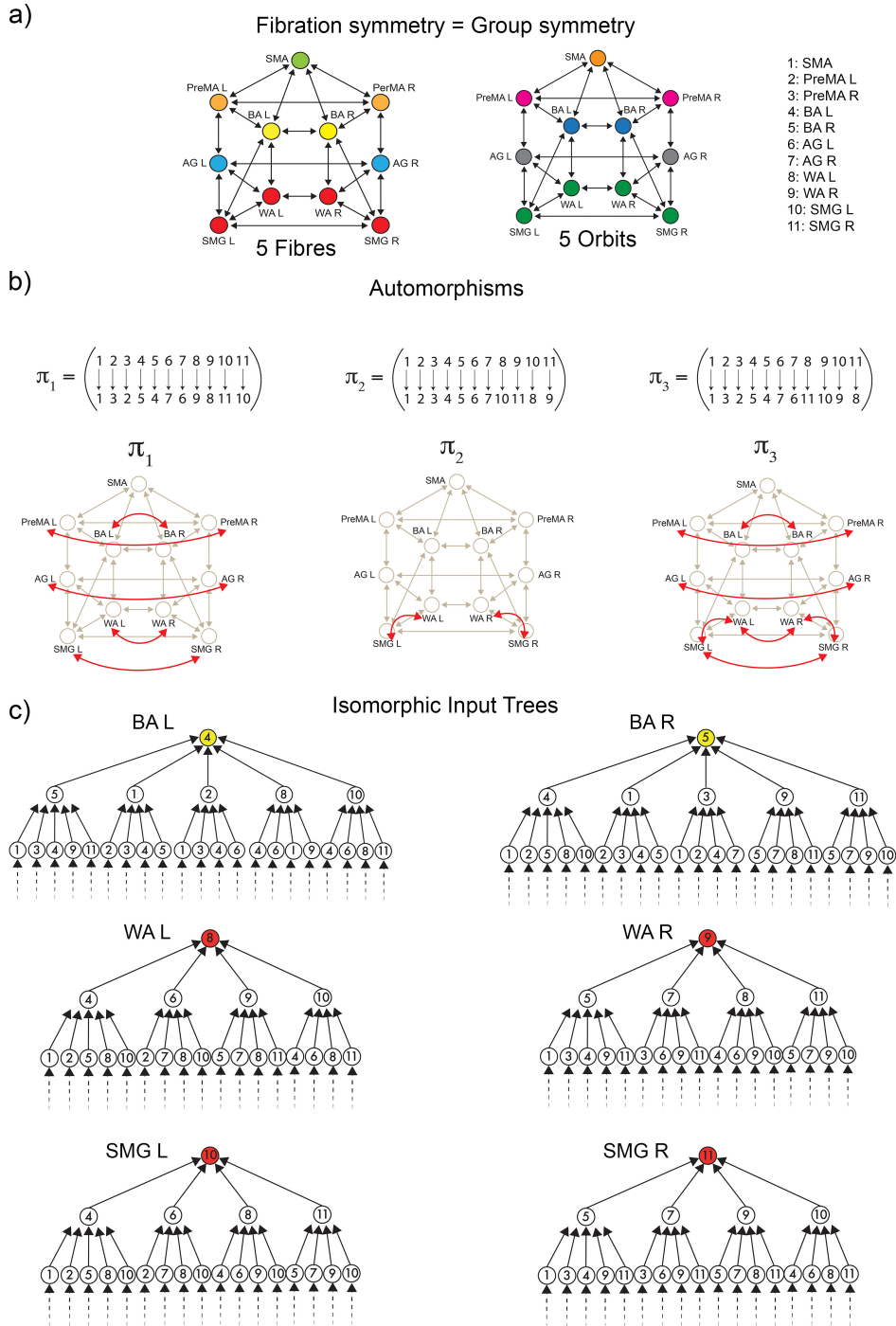


Figure 7: **Extended Data Fig. 7. Group and fibration symmetry analysis of the dual stream (dorsal) baseline connectome of language.** (a) Orbital and fiber partition of this connection is the same, indicating a high level of symmetry of the 'highway' network. (b) Two generators of the symmetry group of the baseline connectome. Left: the left-right (mirror) global symmetry  $\pi_1$ . Center: the symmetry permutation  $\pi_2 = (WAL\ SMG_L)(WAR\ SMG_R)$ . Applying these two symmetries to each node in the graph generates the orbits. Right: composition between  $\pi_3 = \pi_1 \cdot \pi_2$ . (c) Example of two sets of isomorphic input trees giving rise to the main fiber made of four ROIs WA and SMG left and right, and one sample of the bilateral fiber BA left and right (the remaining bilateral fibers are similar). This graph has the same group and fibration symmetry.

## Symmetry analysis of inferred resting state structural network

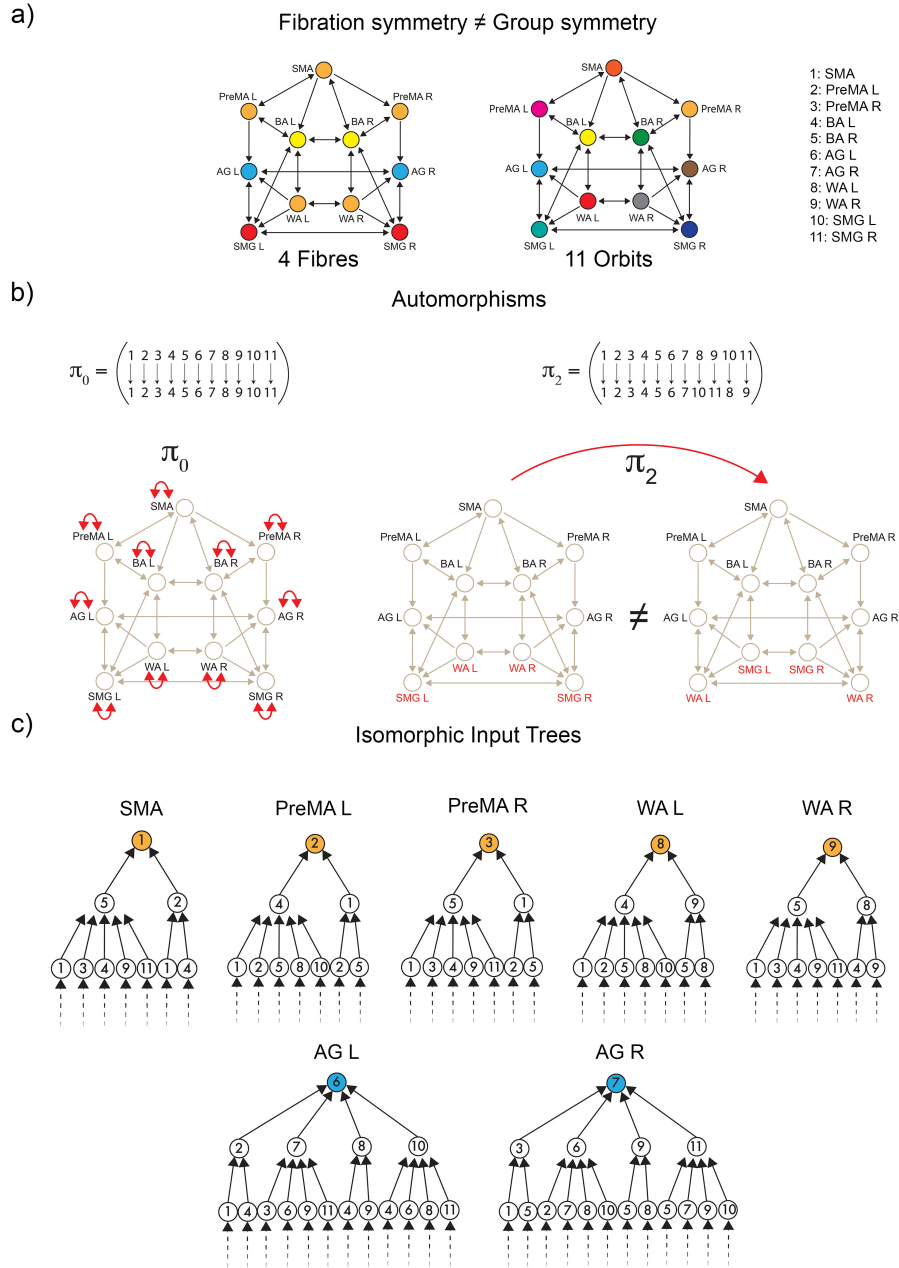


Figure 8: **Extended Data Fig. 8. Group and fibration symmetry analysis of the inferred structural network supporting the resting state.** (a) Orbital and fiber partition of the structural network. This network has no automorphisms, except for the trivial identity leading to a trivial orbital partition of 11 colors where each ROI is its own (trivial) orbit. This implies that the symmetry group of the underlying baseline connectome of Fig. 7a has been completely broken in the resting state. However, the fibration symmetry remains. Fibration analysis reveals four fibers as observed in the four balanced colorings of the network. (b) There are no (non-trivial) automorphisms in this network. Only the identity  $\pi_0$  is a trivially global symmetry (left). The permutation  $\pi_2$  showing in the right is not a symmetry. Yet, WA left and right are still locally symmetric under a fibration. (c) Example of isomorphic input trees of the ROIs in the main fiber made of the pentagonal fiber: PreMA left and right, SMA and WA left and right, and one sample of the bilateral fiber AG left and right (the remaining bilateral fibers are similar).

## Symmetry analysis of inferred language structural network

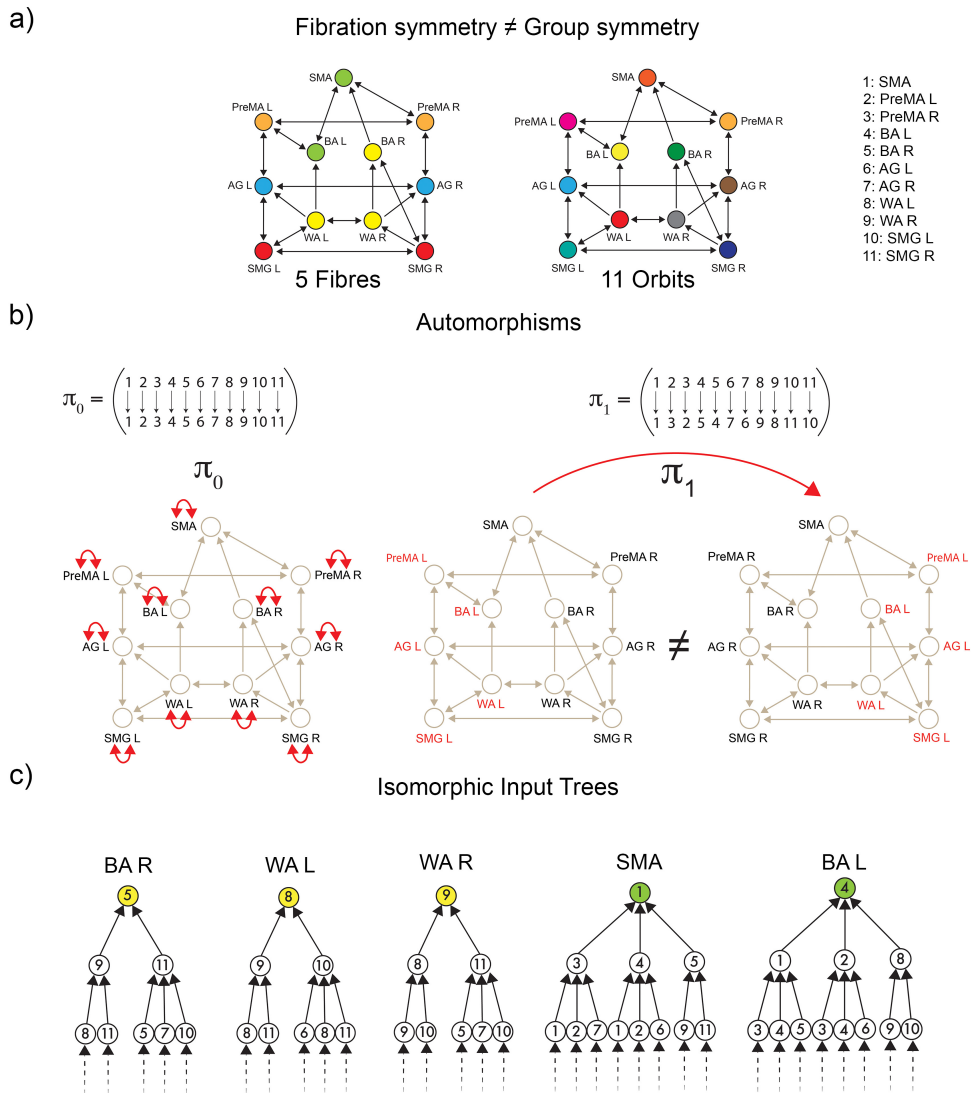


Figure 9: **Extended Data Fig. 9. Group and fibration symmetry analysis of the inferred structural network supporting the language task.** (a) Orbital and fiber partition of the structural network. This network has no automorphisms, except for the identity leading to a trivial orbital partition of 11 colors where each ROI is its own (trivial) orbit. The symmetry group of the resting state network of Fig. 8a remains fully broken in the task. The local fibration symmetry is broken from the resting state due to the lateralization imposed by the task. BA left, and right are broken, and they are recruited by the SMA and WA, respectively, belonging now to two different fibers (colors). The number of fibers is now five, implying a broken fibration symmetry from the resting state since there are more fibers (less symmetry) in the task. (b) Like in the resting state, this network has no (non-trivial) automorphisms. For instance, the global left-right group symmetry is broken, as the figure indicates. (c) Example of isomorphic input trees of the ROIs in the largest fiber made of the three ROIs: WA left and right, and BA right, and the fiber formed by SMA and BA left.